Fermi liquid instabilities in the spin channel

Congjun Wu,[1] Kai Sun,[2] Eduardo Fradkin,[2] and Shou-Cheng Zhang[3]

[1]*Kavli Institute for Theoretical Physics, University of California, Santa Barbara, California 93106-4030, USA*

[2]*Department of Physics, University of Illinois at Urbana-Champaign, Urbana, Illinois 61801-3080, USA*

[3]*Department of Physics, McCullough Building, Stanford University, Stanford, California 94305-4045, USA*

We study the Fermi-surface instabilities of the Pomeranchuk type [Sov. Phys. JETP **8**, 361 (1959)] in the spin-triplet channel with high orbital partial waves [$F_l^a(l>0)$]. The ordered phases are classified into two classes, dubbed the α and β phases by analogy to the superfluid ^{3}He A and B phases. The Fermi surfaces in the α phases exhibit spontaneous anisotropic distortions, while those in the β phases remain circular or spherical with topologically nontrivial spin configurations in momentum space. In the α phase, the Goldstone modes in the density channel exhibit anisotropic overdamping. The Goldstone modes in the spin channel have a nearly isotropic underdamped dispersion relation at small propagating wave vectors. Due to the coupling to the Goldstone modes, the spin-wave spectrum develops resonance peaks in both the α and β phases, which can be detected in inelastic neutron-scattering experiments. In the p-wave channel β phase, a chiral ground-state inhomogeneity is spontaneously generated due to a Lifshitz-like instability in the originally nonchiral systems. Possible experiments to detect these phases are discussed.

I. INTRODUCTION

The Landau theory of the Fermi liquid is one of the most successful theories of condensed-matter physics.[1,2] It describes a stable phase of dense interacting fermionic systems, a *Fermi liquid* (FL). The Fermi liquid theory is the foundation of our understanding of conventional, weakly correlated, metallic systems. Its central assumption is the existence of well-defined fermionic quasiparticles, single-particle fermionic excitations, which exist as long-lived states at very low energies, close enough to the Fermi surface. In the Landau theory, the interactions among quasiparticles are captured by a few Landau parameters $F_l^{s,a}$, where l denotes the orbital angular momentum partial-wave channel, and s,a denote spin-singlet and -triplet channels, respectively. Physical quantities, such as the spin susceptibility, and properties of collective excitations, such as the dispersion relation of zero sound collective modes, acquire significant but finite renormalizations due to the Landau interactions. In the FL phase, except for these finite renormalizations, the effects of the interactions become negligible at asymptotically low energies. It has, however, long been known that the stability of the FL requires that the Landau parameters cannot be too negative, $F_l^{s,a}>-(2l+1)$, a result derived by Pomeranchuk.[3] The most familiar of these Pomeranchuk instabilities are found in the s-wave channel: the Stoner ferromagnetism at $F_0^a<-1$ and phase separation at $F_0^s<-1$.

It has been realized quite recently that when these bounds are violated in a channel with a nonvanishing angular momentum, there is a ground-state instability in the particle-hole and spin-single channel, leading to a spontaneous distortion of the Fermi surface. This is a quantum phase transition to a uniform but anisotropic liquid phase of the fermionic system.[4] In such a phase the electron fluid behaves, from the point of view of its symmetries and of their breaking, very much like an electronic analog of liquid-crystal phases.[5,6] The charge nematic is the simplest example

of such electronic liquid-crystal phases, a concept introduced in Ref. 7 to describe the complex phases of strongly correlated systems such as doped Mott insulators. The charge nematic phase has also been suggested to exist in the high T_c materials near the melting of the (smectic) stripe phases,[7,8] and in quantum Hall systems in nearly half-filled Landau levels.[9,10] Experimentally, the charge nematic phase has been found in ultrahigh mobility two-dimensional electron gases (2DEGs) in AlAs-GaAs heterostructures and quantum wells in large magnetic fields, in nearly half-filled Landau levels for $N \geqslant 2$ at very low temperatures.[10–13] Strong evidence for a charge nematic phase has been found quite recently near the metamagnetic transition of the ultraclean samples of the bilayer ruthenate $Sr_3Ru_2O_7$.[14,15]

Electronic liquid-crystal phases can also be realized as Pomeranchuk instabilities in the particle-hole channel with nonzero angular momentum. This point of view has been the focus of much recent work, both in continuum system[4,16–19] as well as in lattice systems,[20–24] in which case these quantum phase transitions involve the spontaneous breaking of the point symmetry group of the underlying lattice. The two-dimensional (2D) quantum nematic Fermi fluid phase is an instability in the d-wave ($l=2$) channel exhibiting a spontaneous elliptical distortion of the Fermi surface.[4] In all cases, these instabilities typically result in anisotropic Fermi-surface distortions, sometimes with a change of the topology of the Fermi surface. Nematic phases also occur in strong coupling regimes of strongly correlated systems such as the Emery model of the high-temperature superconductors.[25] If lattice effects are ignored, the nematic state has Goldstone modes, which can be viewed as the rotation of the distorted Fermi surface, i.e., the soft Fermi-surface fluctuations. Within a random-phase-approximation (RPA) approach,[4] confirmed by a nonperturbative high-dimensional bosonization treatment,[17] the Goldstone modes were shown to be overdamped in almost all the propagating directions, except along the high-symmetry axes of the distorted Fermi surface.

The Goldstone mode couples strongly to electrons, giving rise to a non-Fermi-liquid behavior throughout the nematic Fermi fluid phase:[4,26] in the perturbation theory, the imaginary part of the electron self-energy is found to be proportional to $\omega^{2/3}$ on most of the Fermi surface, except along four "nodal" directions, leading to the breakdown of the quasiparticle picture. Away from the quantum critical point, this effect is suppressed by lattice effects but it is recovered at quantum criticality[21] and at high temperatures (if the lattice pinning effects are weak). Beyond perturbation theory,[26] this effect leads to a form of "local quantum criticality."

Richer behaviors can still be found in Pomeranchuk instabilities in the spin triplet and $l>0$ angular momentum channels.[4,8,27–34] Typically, this class of instabilities breaks both the spatial (orbital) and spin SU(2) rotation symmetries. A p-wave channel instability was studied by Hirsch.[27,28] The Fermi surfaces of spin-up and -down components in such a state shift along opposite directions. The p-wave channel instability was also proposed by Varma[31] and Varma and Zhu[32] as a candidate for the hidden order appearing in the heavy fermion compound URu_2Si_2 below 17 K. Gor'kov and Sokol studied the non-Néel spin orderings in itinerant systems and showed their relation to the Pomeranchuk instability.[29] In Refs. 4 and 8 a nematic-spin-nematic phase was proposed, nematic state in both real space and in the internal spin space, where the two Fermi surfaces of up and down spins are spontaneously distorted into two orthogonal ellipses. Podolsky and Demler[35] considered a spin-nematic phase as arising from the melting of a stripe phase; this phase can also be a nematic-spin-nematic if it retained a broken rotational symmetry, as expected from the melting of a stripe (or smectic) phase.[7,36] Kee and Kim[33] have suggested a state to explain the behavior of $Sr_3Ru_2O_7$, which can be shown to be a lattice version of a partially polarized nematic-spin-nematic state.

Interestingly, the spin-triplet Pomeranchuk instabilities can also occur without breaking rotational invariance in real space, and keep the symmetries of the undistorted Fermi surface. Wu and Zhang[30] showed that a state of this sort can exist in the p-wave channel, with the distortions affecting only the spin channel. In this state, there are two Fermi surfaces with different volumes, as in ferromagnetic systems. Although both the spatial and spin rotation symmetries are broken, a combined spin-orbit rotation keeps the system invariant; i.e., the total angular momentum is conserved. The broken symmetry in such a state is the relative spin-orbit symmetry, which was proposed by Leggett in the context of superfluid ^{3}He B phase.[1] In fact, it is a particle-hole channel analog of the superfluid ^{3}He B phase, where the pairing gap function is isotropic over the Fermi surface. The phases with anisotropic Fermi-surface distortions are the analog of the ^{3}He A phase, where the gap function is anisotropic. The two possibilities of keeping or breaking the shape of Fermi surfaces are dubbed β and α phases, respectively, by analogy with B and A superfluid phases in ^{3}He systems. An important difference is, however, that while in the A and B phases of superfluid ^{3}He, all the Fermi surface is gapped, up to a set of measure zero of nodal points in the A phase, in the β and α phases of spin-triplet Pomeranchuk systems no gap in the fermionic spectrum ever develops.

An important common feature of the α and β phases is the dynamical appearance of effective spin-orbit (SO) couplings, reflecting the fact that in these phases spin and orbit degrees of freedom become entangled.[37] Conventionally, in atomic physics, the SO coupling originates from leading-order relativistic corrections to the Schrödinger-Pauli equation. As such, the standard SO effects in many-body systems have an inherently single-particle origin, and are unrelated to many-body correlation effects. The Pomeranchuk instabilities involving spin we are discussing here thus provide a different mechanism to generate effective SO couplings through phase transitions in a many-body nonrelativistic system. In the 2D β phase, both Rashba-like and Dresselhaus-like SO couplings can be generated. In the α phase, the resulting SO coupling can be considered as a mixture of Rashba and Dresselhaus with equal coupling strengths. Such SO coupling systems could, in principle, be realized in 2D semiconductor materials, leading to interesting effects. For instance, a hidden SU(2) symmetry in such systems was found to give rise to a long-lived spin spiral excitation with the characteristic wave vector relating the two Fermi surfaces together.[38] Recently, many proposals have been suggested to employ SO coupling in semiconductor materials to generate spin current through electric fields. The theoretical prediction of this "intrinsic spin Hall effect"[39,40] has stimulated tremendous research activity both theoretical and experimental.[41,42] Thus, Pomeranchuk instabilities in the spin channel may have a potential application for the field of spintronics.

A systematic description of the high partial-wave channel Pomeranchuk instabilities involving spin is still lacking in the literature. In this paper, we investigate this problem for arbitrary orbital partial-wave channels in two dimensions, and for simplicity only in the p-wave channel in three dimensions. We use a microscopic model to construct a general Ginzburg-Landau (GL) free energy to describe these instabilities, showing that the structure of the α and β phases are general for arbitrary values of l. The α phases exhibit anisotropic relative distortions for two Fermi surfaces, as presented in previous publications. We also investigate the allowed topological excitations (textures) of these phases and find that a half-quantum vortexlike defect in real space combined with spin-orbit distortions. The β phases at $l\geqslant 2$ also have a vortex configuration in momentum space with winding numbers $\pm l$, which are equivalent to each other by a symmetry transformation.

We study the collective modes in the critical regime and in the ordered phases at zero temperature. At the quantum critical point, as in the cases previously studied, the theory has the dynamic critical exponent $z=3$ for all values of the orbital angular momentum l. In the anisotropic α phase, the Goldstone modes can be classified into density and spin channel modes, respectively. The density channel Goldstone mode exhibits anisotropic overdamping in almost all the propagating directions. In contrast, the spin channel Goldstone modes show nearly isotropic underdamped dispersion relation at small propagating wave vectors. In the β phase, the Goldstone modes are relative spin-orbit rotations which have linear dispersion relations at $l\geqslant 2$, in contrast to the quadratic spin-wave dispersion in the ferromagnet. Both the Goldstone modes (spin channel) in the α phases and the

relative spin-orbit Goldstone modes in the β phases couple to spin excitations in the ordered phases. Thus, the spin-wave spectra develop characteristic resonance peaks observable in neutron-scattering experiments, which are absent in the normal phase.

The p-wave channel Pomeranchuk instability involving spin is special because the GL free energy contains a cubic term of order parameters with a linear spatial derivative satisfying all the symmetry requirements. Such a term is not allowed in other channels with $l \neq 1$, including the ferromagnetic instability and the Pomeranchuk instabilities in the density channel. This term does not play an important role in the α phase, but in the β phase, it induces a chiral inhomogeneous ground-state configuration, leading to a Lifshitz-like instability in this originally nonchiral system. In other words, a Dzyaloshinskii-Moriya-type interaction for the Goldstone modes is generated in the β phase. The effect bears some similarity to the helimagnet[43] and chiral liquid crystal[6] except that the parity is explicitly broken there but not here. The spiral pattern of the ground-state order parameter is determined.

The paper is organized as follows: In Sec. II, we construct the model Hamiltonian for the Pomeranchuk instabilities with spin. In Sec. III, we present the Ginzburg-Landau free-energy analysis to determine the allowed ground states. In Sec. IV, we discuss the results of the mean-field theory. In Sec. V, we discuss the topology of the broken-symmetry states and classify the topological defects. In Sec. VI, we calculate the collective modes at the critical point at zero temperature. In Secs. VII and VIII, we investigate the Goldstone modes in the α and β phases, respectively, and study the spontaneous Lifshitz instability in the β phase at $l=1$. In Sec. IX, we present the magnetic-field effects. In Sec. X, we show that in the α and β phases in the quadrupolar channel ($l=2$), a spin current can be induced when a charge current flows through the system. In Sec. XI, we discuss the possible experimental evidence for Pomeranchuk instabilities involving spins. We summarize the results of this paper in Sec. XII. Details of our calculations are presented in two appendixes. In Appendix A, we specify our conventions for Landau parameters, and in Appendix B, we give details of the Goldstone modes for spin oscillations in the α phase.

II. MODEL LANDAU HAMILTONIAN

We begin with the model Hamiltonian describing the Pomeranchuk instability in the F_l^a ($l \geq 1$) channel in 2D. Later on in the paper, we will adapt this scheme to discuss the three-dimensional (3D) case, which is more complex. This model, and the related model for the spin-singlet sector of Ref. 4 on which it is inspired, has the same structure as the effective Hamiltonian for the Landau theory of a FL. The corresponding order parameters can be defined through the matrix, form as

$$Q^{\mu b}(r) = \psi_\alpha^\dagger(r) \sigma_{\alpha\beta}^\mu g_{l,b}(-i\hat{\nabla}) \psi_\beta(r), \qquad (2.1)$$

where the Greek index μ denotes the x, y, z directions in the spin space, in two dimensions the Latin index $b=1,2$ denotes

the two orbital components, and $\alpha, \beta = \uparrow, \downarrow$ label the two spin projections. (Hereafter, repeated indices are summed over.) In two dimensions, the operators $g_{l,1} \pm i g_{l,2}$, which carry the azimuthal angular momentum quantum number $L_z = \pm l$, are given by

$$g_{l,1}(-i\hat{\nabla}) \pm i g_{l,2}(-i\hat{\nabla}) = (-i)^l (\hat{\nabla}_x \pm i\hat{\nabla}_y)^l, \qquad (2.2)$$

where the operator $\hat{\nabla}^a$ is defined as $\vec{\nabla}^a / |\nabla|$. The 3D counterpart of these expressions can be written in terms of spherical harmonic functions. Thus, in three dimensions the Latin labels take $2l+1$ values. For the moment, and for simplicity, we will first discuss the 2D case.

In momentum space (i.e., a Fourier transform), we can write the operators of Eq. (2.2) in the form $g_{l,1}(\vec{k}) = \cos l\theta_k$ and $g_{l,2}(\vec{k}) = \sin l\theta_k$, where θ_k is the azimuthal angle of $\vec{k}$ in the 2D plane. In momentum space, $Q^{\mu b}(\vec{q})$ is defined as

$$Q^{\mu b}(\vec{q}) = \sum_{\vec{k}} \psi_\alpha^\dagger\left(\vec{k} + \frac{\vec{q}}{2}\right) \sigma_{\alpha\beta}^\mu g_{l,b}(\vec{k}) \psi_\beta\left(\vec{k} - \frac{\vec{q}}{2}\right). \quad (2.3)$$

It satisfies $Q^{\mu b}(-\vec{q}) = Q^{\mu b *}(\vec{q})$; thus, $Q^{\mu b}(\vec{r})$ is real.

We generalize the Hamiltonian studied in Refs. 4 and 30 to the F_l^a channel with arbitrary values of l as

$$H = \int d^2\vec{r} \psi_\alpha^\dagger(\vec{r})[\epsilon(\vec{\nabla}) - \mu]\psi_\alpha(\vec{r}) + \frac{1}{2}\int d^d\vec{r} d^d\vec{r}' f_l^a(\vec{r} - \vec{r}')$$
$$\times \sum_{\mu b} \hat{Q}^{\mu b}(\vec{r})\hat{Q}^{\mu b}(\vec{r}'), \qquad (2.4)$$

where μ is the chemical potential. For later convenience, we include the nonlinear momentum dependence in the single-particle spectrum up to the cubic level as

$$\epsilon(\vec{k}) = v_F \Delta k[1 + a(\Delta k/k_F) + b(\Delta k/k_F)^2 + \cdots], \quad (2.5)$$

with $\Delta k = k - k_F$. Here, v_F and k_F are the Fermi velocity and the magnitude of the Fermi wave vector in the FL.

The Fourier transform of the Landau interaction function $f(r)$ is

$$f(\vec{q}) = \int d\vec{r} e^{i\vec{q}\vec{r}} f_l^a(r) = \frac{f_l^a}{1 + \kappa|f_l^a|q^2}, \qquad (2.6)$$

and the dimensionless Landau parameters are defined as

$$F_l^a = N(0)f_l^a(q=0), \qquad (2.7)$$

with $N(0)$ the density of states at the Fermi energy. This Hamiltonian possesses the symmetry of the direct product of $SO_L(2) \otimes SO_S(3)$ in the orbit and spin channels.

The Landau-Pomeranchuk (LP) instability occurs at $F_l^a < -2$ at $l \geq 1$ in two dimensions. For the general values of l, we represent the order parameter by a 3×2 matrix,

$$n^{\mu,b} = |f_l^a| \int \frac{d^2\vec{k}}{(2\pi)^2} \langle \psi_\alpha^\dagger(\vec{k}) \sigma_{\alpha\beta}^\mu g_{l,b}(\vec{k}) \psi_\beta(\vec{k}) \rangle. \qquad (2.8)$$

It is more convenient to represent each column of the matrix form $n^{\mu,b}$ ($b=1,2$) as a 3-vector in spin space as

$$\vec{n}_1 = n^{\mu,1}, \quad \vec{n}_2 = n^{\mu,2}. \tag{2.9}$$

For $l=1$, $\vec{n}_{1,2}$ are just the spin currents along the x,y directions, respectively. When $l \geq 2$, $\vec{n}_{1,2}$ denote the spin multipole components at the level l on the Fermi surface. $\vec{n}_1 \pm i\vec{n}_2$ carry the orbital angular momenta $L_z = \pm l$, respectively. In other words, $\vec{n}_{1,2}$ are the counterpart of the spin moment in the lth partial-wave channel in momentum space.

The mean-field Hamiltonian, i.e., for a state with a uniform order parameter, can be decoupled as

$$H_{\mathrm{MF}} = \int \frac{d^2\vec{k}}{(2\pi)^2} \psi_\alpha^\dagger(\vec{k}) \{\epsilon(\vec{k}) - \mu - [\vec{n}_1 \cos(l\theta_k)$$
$$+ \vec{n}_2 \sin(l\theta_k)] \cdot \vec{\sigma}\} \psi_\beta(\vec{k}) + \frac{|n_1|^2 + |n_2|^2}{2|f_l^a|}. \tag{2.10}$$

This mean-field theory is valid when the interaction range $\xi \approx \sqrt{\kappa|f_l^a|}$ is much larger than the interparticle distance $d \approx 1/k_F$. The actual validity of mean-field theory at quantum criticality requires an analysis of the effects of quantum fluctuations, which are not included in the mean-field theory.[44,45] In this theory, just as the case of Ref. 4, the dynamic critical exponent turns out to be $z=3$ and the mean-field theory appears to hold even at quantum criticality.

Taking into account that $|f_1^a| \sim 1/N(0)$ around the transition point, we introduce a dimensionless parameter λ to denote the above criterion as

$$\lambda = \frac{\kappa k_F^2}{N(0)} \gg 1. \tag{2.11}$$

Finally, notice that, in the p-wave channel, the Hamiltonian [Eq. (2.10)] can be formally represented through an SU(2) non-Abelian gauge field minimally coupled to the fermions,

$$H_{\mathrm{MF}} = \int d^2\vec{r} \frac{1}{2m} \psi^\dagger(\vec{r})[-i\hbar\nabla^a - mA_a^\mu(\vec{r})\sigma^\mu]^2 \psi(\vec{r})$$
$$- \frac{m}{2} \psi^\dagger(\vec{r})\psi(\vec{r})A_a^\mu(\vec{r})A_a^\mu(\vec{r}), \tag{2.12}$$

where the gauge field is defined as

$$A_a^\mu(\vec{r})\sigma^\mu = n^{\mu a}(\vec{r})\sigma^\mu. \tag{2.13}$$

Notice, however, that this is an approximate effective local gauge invariance, which only holds for a theory with a *linear dispersion relation*, and that it is manifestly broken by nonlinear corrections, such as the quadratic term of Eq. (2.12) and the cubic terms included in the dispersion $\epsilon(\vec{k})$ of Eq. (2.5).

III. GINZBURG-LANDAU FREE ENERGY

A. 2D systems

In order to analyze the possible ground-state configuration discussed in Sec. I, we construct the GL free energy in two dimensions in the arbitrary l-wave channel. The symmetry constraint to the GL free energy is as follows. Under time-reversal (TR) and parity transformations, $\vec{n}_{1,2}$ transform, respectively, as

$$T\vec{n}_{1,2}T^{-1} = (-)^{l+1}\vec{n}_{1,2}, \quad P\vec{n}_{1,2}P^{-1} = (-)^l\vec{n}_{1,2}. \tag{3.1}$$

Under the $SO_S(3)$ rotation $R_{\mu\nu}$ in the spin channel, $\vec{n}_{1,2}$ transform as

$$n_{\mu,1} \rightarrow R_{\mu\nu}n_{\nu,1}, \quad n_{\mu,2} \rightarrow R_{\mu\nu}n_{\nu,2}, \tag{3.2}$$

On the other hand, under a uniform rotation by an angle θ about the z axis, in the orbital channel, the order parameters $\vec{n}_a$ transform as

$$\vec{n}_1 \rightarrow \cos(l\theta)\vec{n}_1 + \sin(l\theta)\vec{n}_2,$$
$$\vec{n}_2 \rightarrow -\sin(l\theta)\vec{n}_1 + \cos(l\theta)\vec{n}_2. \tag{3.3}$$

Thus, the order-parameter fields $\vec{n}_1$ and $\vec{n}_2$ are invariant under spatial rotations by $2\pi/l$ and change sign under a rotation by π/l. In the α phase, this change can be compensated by flipping the spins.

In order to maintain the $SO_L(2) \otimes SO_S(3)$ symmetry, up to quartic terms in the order-parameter fields $\vec{n}_a$, the uniform part of the GL free energy has the form,

$$F(n) = r\,\mathrm{tr}(n^T n) + \left(v_1 + \frac{v_2}{2}\right)[\mathrm{tr}(n^T n)]^2 - \frac{v_2}{2}\mathrm{tr}[(n^T n)^2]$$
$$= r(|\vec{n}_1|^2 + |\vec{n}_2|^2) + v_1(|\vec{n}_1|^2 + |\vec{n}_2|^2)^2 + v_2|\vec{n}_1 \times \vec{n}_2|^2. \tag{3.4}$$

The coefficients r, v_1, and v_2 will be presented in Eq. (4.12) by evaluating the ground-state energy of the mean-field Hamiltonians [Eqs. (4.1) and (4.7)]. The Pomeranchuk instability occurs at $r<0$, i.e., $F_l^a < -2(l \geq 1)$. Furthermore, for $v_2 > 0$, the ground state is the α phase, which favors $\vec{n}_1 \| \vec{n}_2$, while leaving the ratio of $|\vec{n}_1|/|\vec{n}_2|$ arbitrary. On the other hand, for $v_2 < 0$ we find a β phase, which favors $\vec{n}_1 \perp \vec{n}_2$ and $|\vec{n}_1| = |\vec{n}_2|$.

The gradient terms are more subtle. We present the gradient terms of the GL free energy for $l=1$ as follows:

$$F_{grad}(n) = \gamma_1 \,\mathrm{tr}[\partial_a n^T \partial_a n] + \gamma_2 \epsilon_{\mu\nu\lambda} n^{\mu a} n^{\nu b} \partial_a n^{\lambda b}$$
$$= \gamma_1(\partial_a \vec{n}_b \cdot \partial_a \vec{n}_b) + \gamma_2[(\partial_x \vec{n}_2 - \partial_y \vec{n}_1) \cdot (\vec{n}_1 \times \vec{n}_2)]. \tag{3.5}$$

For simplicity, as in Ref. 4, we have neglected the difference between two Franck constants and only present one stiffness coefficient γ_1. (This approximation is accurate only near the Pomeranchuk quantum critical point.) More importantly, because $n^{\mu,b}$ is odd under parity transformation for $l=1$, a new γ_2 term appears, which is of cubic order in the order-parameter field $n^{\mu,b}$, and it is linear in derivatives. This term is allowed by all the symmetry requirements, including time reversal, parity, and rotation symmetries. This term has no important effects in the disordered phase and in the α phase, but it leads to a Lifshitz-like inhomogeneous ground state with spontaneous chirality in the β phase, in which parity is spontaneously broken. We will discuss this effect in detail in Sec. VIII. The coefficient of $\gamma_{1,2}$ will be presented in Eq. (8.19). Similarly, for all the odd values of l, we can write a real cubic γ_2 term satisfying all the symmetry constraints as

$$\gamma_2 \epsilon_{\mu\nu\lambda} n^{\mu a} n^{\nu b} (i)^l g_a(\hat{\nabla}) n^{\lambda b}. \tag{3.6}$$

However, this term corresponds to high-order corrections, and is negligible (irrelevant) for $l \geq 3$.

Similar to the approximate gauge symmetry for the fermions in Eq. (2.12), the γ_2 term can also be reproduced by a non-Abelian gauge potential defined as

$$i A_a^\lambda(x)(T^\lambda)_{\mu\nu} = \epsilon_{\lambda\mu\nu} n^{\lambda a}(x), \tag{3.7}$$

where $T_{\mu\nu}^\lambda = -i\epsilon_{\lambda\mu\nu}$ is the generator of the SU(2) gauge group in the vector representation. Then, Eq. (3.5) can be written as

$$
\begin{aligned}
F_{grad}(n) &= \gamma_1 \{ [\partial_a \delta_{\mu\nu} - i g A_a^\lambda (T^\lambda)_{\mu\nu}] n^{\nu b} \}^2 + \gamma_1 g^2 (\epsilon_{\lambda\mu\nu} n^{\lambda a} n^{\nu b})^2 \\
&= \sum_{ab} [\gamma_1 (\partial_a \vec{n}_b + g\vec{n}_a \times \vec{n}_b)^2 - \gamma_1 g^2 |\vec{n}_a \times \vec{n}_b|^2], \quad (3.8)
\end{aligned}
$$

with $g = \gamma_2/(2\gamma_1)$

B. 3D systems

In three dimensions, the order parameter in the F_l^a channel Pomeranchuk instabilities can be similarly represented by a $3 \times (2l+1)$ matrix. Here we only consider the simplest case of the p-wave channel instability ($l=1$), which has been studied in Refs. 4, 27, 30, and 32 under different contexts. In the F_1^a channel, the order parameter $n^{\mu,i}$ is a 3×3 real matrix defined as

$$n^{\mu,b} = |f_1^a| \int \frac{d^3\vec{k}}{(2\pi)^3} \langle \psi_\alpha^\dagger(k) \sigma_{\alpha\beta}^\mu k^b \psi_\beta(k) \rangle. \tag{3.9}$$

The difference between $n^{\mu,i}$ and the triplet p-wave pairing order parameter in the ^{3}He system[1,46] is that the former is defined in the particle-hole channel, and thus is real. By contrast, the latter one is defined in the particle-particle channel and is complex. Each column of the matrix form $n^{\mu,b}$ ($b = x, y, z$) can be viewed as a 3-vector in the spin space as

$$\vec{n}_1 = n^{\mu,1}, \quad \vec{n}_2 = n^{\mu,2}, \quad \vec{n}_3 = n^{\mu,3}, \tag{3.10}$$

which represents the spin current in the x, y, and z directions, respectively. The GL free energy in Ref. 30 can be reorganized as

$$
\begin{aligned}
F(n) &= r\, \mathrm{tr}(n^T n) + \left(v_1' + \frac{v_2'}{2} \right) [\mathrm{tr}(n^T n)]^2 - \frac{v_2'}{2} \mathrm{tr}[(n^T n)^2] \\
&= r'(|\vec{n}_1|^2 + |\vec{n}_2|^2 + |\vec{n}_3|^2) + v_1'(|\vec{n}_1|^2 + |\vec{n}_2|^2 + |\vec{n}_3|^2)^2 \\
&\quad + v_2'(|\vec{n}_1 \times \vec{n}_2|^2 + |\vec{n}_2 \times \vec{n}_3|^2 + |\vec{n}_3 \times \vec{n}_1|^2), \quad (3.11)
\end{aligned}
$$

where the coefficients r', $v_{1,2}'$ will be presented in Eq. (4.19). Similarly, the α phase appears at $v_2 > 0$, which favors that $\vec{n}_1 \| \vec{n}_2 \| \vec{n}_3$ and leaves their ratios arbitrary. The β phase appears at $v_2 < 0$, which favors that vectors $\vec{n}_{1,2,3}$ are perpendicular to each other with equal amplitudes $|\vec{n}_1| = |\vec{n}_2| = |\vec{n}_3|$.

Similarly, we present the gradient terms in the GL free energy as

$$F_{grad}(n) = \gamma_1' \, \mathrm{tr}[\partial_a n^T \partial_a n] + \gamma_2' \epsilon_{\mu\nu\lambda} n^{\mu i} n^{\nu j} \partial_j n^{\lambda i}, \tag{3.12}$$

where the coefficient $\gamma_{1,2}'$ will be presented in Eq. (8.36). Again, we neglect the difference among three Franck constants. The γ_2' term can be represented as
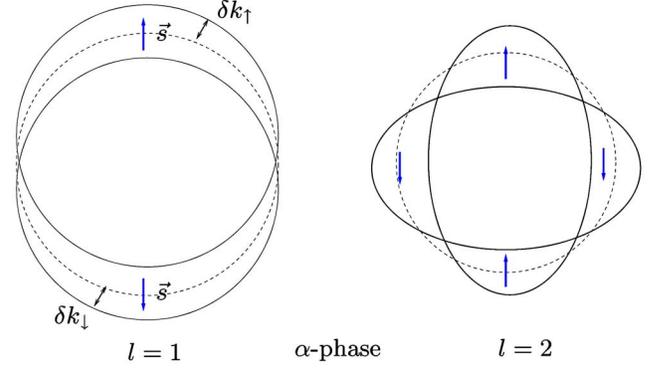

FIG. 1. (Color online) The α phases in the F_1^a and F_2^a channels. The Fermi surfaces exhibit the p- and d-wave distortions, respectively.

$$
\begin{aligned}
\gamma_2' [& (\partial_x \vec{n}_2 - \partial_y \vec{n}_1) \cdot (\vec{n}_1 \times \vec{n}_2) + (\partial_y \vec{n}_3 - \partial_z \vec{n}_2) \cdot (\vec{n}_2 \times \vec{n}_3) \\
& + (\partial_z \vec{n}_1 - \partial_x \vec{n}_3) \cdot (\vec{n}_3 \times \vec{n}_1)]. \tag{3.13}
\end{aligned}
$$

It can also be represented in terms of the non-Abelian gauge potential as in Eq. (3.8).

IV. MEAN-FIELD PHASES IN THE F_l^a CHANNEL

In this section, we discuss the solution to the mean-field Hamiltonian [Eq. (2.10)] for the ordered α and β phases in both two and three dimensions.

A. 2D α phases

The α phase is characterized by an anisotropic distortion of the Fermi surfaces of up and down spins. In this phase, s_z is a good quantum number. It is a straightforward generalization of the nematic Fermi liquid for the case of the spin channel.[4] For example, the Fermi-surface structures at $l = 1, 2$ are depicted in Fig. 1. The quadrupolar, $l = 2$, case is the nematic-spin-nematic phase.[4,8] Without loss of generality, we choose $\vec{n}_1 = \bar{n}\hat{z}$ and $|n_2| = 0$. The mean-field Hamiltonian H_α for the α phase becomes

$$H_{\alpha,l} = \int \frac{d^2 k}{(2\pi)^2} \psi^\dagger(\vec{k}) [\epsilon(\vec{k}) - \mu - \bar{n}\cos(l\theta_k)\sigma_z] \psi(\vec{k}). \tag{4.1}$$

The dispersion relations for the spin-up and -down electrons become

$$\xi_{\uparrow,\downarrow}(\vec{k}) = \epsilon(k) - \mu \mp \bar{n}\cos(l\theta_k). \tag{4.2}$$

The value of $\bar{n}$ can be obtained by solving the self-consistent equation in the α phase,

$$\frac{\bar{n}}{|f_l^a(0)|} = \int \frac{d\vec{k}}{(2\pi)^2} [n_f(\xi_\uparrow(\vec{k})) - n_f(\xi_\downarrow(\vec{k}))] \cos(l\theta_k), \tag{4.3}$$

where $n_f(\xi_\uparrow(k))$ and $n_f(\xi_\downarrow(k))$ are the Fermi functions for the up and down electrons, respectively. The distortions of the Fermi-surfaces of the spin-up and spin-down bands are given by an angle-dependent part of their Fermi wave vectors:

$$\frac{\delta k_{F\uparrow,\downarrow}(\theta)}{k_F} = \frac{2a-1}{4}x^2 \pm \left(x + \frac{a-2a^2}{2}x^3\right)\cos l\theta$$
$$- ax^2 \cos^2 l\theta \pm (2a^2-b)x^3 \cos^3 l\theta + O(x^4),$$

$$(4.4)$$

where we introduced the dimensionless parameter x $=\bar{n}/(v_F k_F)$, where v_F and k_F are the Fermi velocity and the magnitude of the Fermi wave vector in the FL phase. This solution holds for small distortions and it is accurate only when close to the quantum phase transition. By inspection, we see that in the α phases the total spin polarization vanishes. More importantly, under a rotation by π/l, the charge and spin components of the order parameter both change sign; i.e., a rotation by π/l is equivalent to a reversal of the spin polarization.

The single-particle fermion Green's function in the α phase at wave vector $\vec{k}$ and Matsubara frequency ω_n is

$$G(\vec{k}, i\omega_n) = \frac{1}{2}\left[\frac{1+\sigma_z}{i\omega_n - \xi_\uparrow(\vec{k})} + \frac{1-\sigma_z}{i\omega_n - \xi_\downarrow(\vec{k})}\right]. \quad (4.5)$$

### B. 2D β phases

The β phase appears for $v_2 < 0$, which favors $\vec{n}_1 \perp \vec{n}_2$ and $|n_1| = |n_2|$. Similar to the case of ferromagnetism, the Fermi surfaces split into two parts with different volumes, while each one still keeps the round shape undistorted. However, an important difference exists between the β phase at $l \geq 1$ and the ferromagnetic phase. In the ferromagnet, the spin is polarized along a fixed uniform direction, which gives rise to a net spin moment. On the other hand, in the β phase with orbital angular momentum $l \geq 1$, *the spin winds around the Fermi surface*, exhibiting a vortexlike structure in momentum space. Consequently, in the β phase the net spin moment is zero, just as it is in the α phase. (Naturally, partially polarized versions of the α and β phases are possible but will not be discussed here.) In other words, it is a spin-nematic, high partial-wave channel generalization of ferromagnetism. In the previously studied cases of the F_1^a channel in Ref. 30, it was shown that in this phase, effective Rashba and Dresselhaus terms are dynamically generated in single-particle Hamiltonians. The ground-state spin configuration exhibits, in momentum space, a vortex structure with winding number $w = \pm 1$ depicted in Fig. 2.

Here, we generalize the vortex picture in momentum space in the F_1^a channel to a general F_l^a channel. We assume $|n_1| = |n_2| = \bar{n}$. Without loss of generality, we can always perform an SO(3) rotation in spin space to set $\vec{n}_1 \| \hat{x}$ and $\vec{n}_2 \| \hat{y}$. Then, much as in the B phase of ^{3}He, the mean-field Hamiltonian $H_{\beta,l}$ for the β phase in angular momentum channel l can be expressed through a d vector, defined by

$$\vec{d}(\vec{k}) = (\cos(l\theta_k), \sin(l\theta_k), 0), \quad (4.6)$$

as follows:
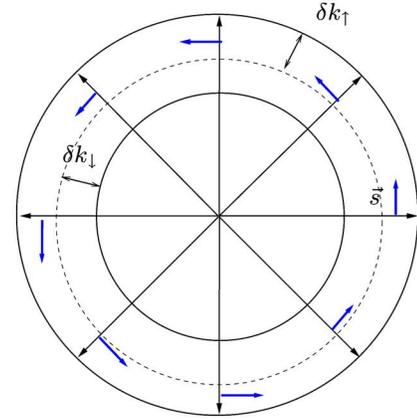
(a) Rashba ($w = 1$)
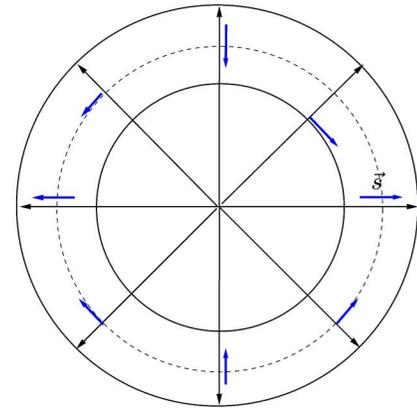
(b) Dresselhaus ($w = -1$)

FIG. 2. (Color online) The β phases in the F_1^a channel. Spin configurations exhibit the vortex structures in the momentum space with winding number $w = \pm 1$, which correspond to Rashba and Dresselhaus SO couplings, respectively.

$$H_{\beta,l} = \int \frac{d^2k}{(2\pi)^2}\psi^\dagger(\vec{k})[\epsilon(\vec{k}) - \mu - \bar{n}\vec{d}(\theta_k)\cdot\vec{\sigma}]\psi(\vec{k}), \quad (4.7)$$

where $\vec{d}(\theta_k)$ is the spin quantization axis for single-particle state at $\vec{k}$. The saddle point value of $\bar{n}$ can be obtained by solving the self-consistent equation,

$$\frac{2\bar{n}}{|f_l^a(0)|} = \int \frac{d^2\vec{k}}{(2\pi)^2}[n_f(\xi_\uparrow(\vec{k})) - n_f(\xi_\downarrow(\vec{k}))], \quad (4.8)$$

where the single-particle spectra read

$$\xi_{\uparrow,\downarrow}(\vec{k}) = \epsilon(\vec{k}) - \mu \pm \bar{n}, \quad (4.9)$$

which is clearly invariant under spatial rotations. The Fermi surface splits into two parts with

$$\frac{\delta k_{F,\uparrow,\downarrow}}{k_F} = \pm x - \frac{x^2}{2} \pm (a-b)x^3 + O(x^4). \quad (4.10)$$

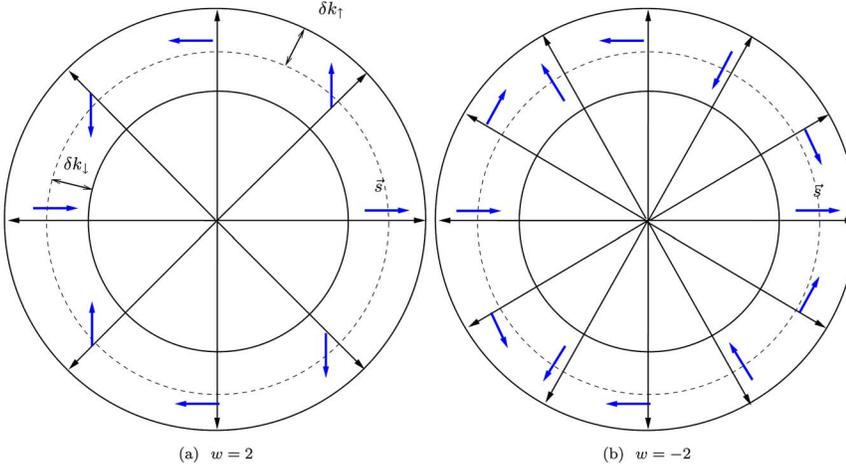The single-particle Green's function in the β phase reads

(a) $w = 2$ (b) $w = -2$

FIG. 3. (Color online) The β phases in the F_2^a channel. Spin configurations exhibit the vortex structure with winding number $w = \pm 2$. These two configurations can be transformed to each other by performing a rotation around the x axis with the angle of π.

$$G(\vec{k}, i\omega_n) = \frac{1}{2}\left[\frac{1 + \vec{\sigma}\cdot\hat{d}}{i\omega_n - \xi_\uparrow(\vec{k})} + \frac{1 - \vec{\sigma}\cdot\hat{d}}{i\omega_n - \xi_\downarrow(\vec{k})} \right], \quad (4.11)$$

where $\vec{\sigma}\cdot\vec{d}(\hat{k})$ is the lth order helicity operator. Each Fermi surface is characterized by the eigenvalues ± 1 of the helicity operators $\vec{\sigma}\cdot\vec{d}(\hat{k})$.

From the mean-field theory of α and β phases, we can calculate the coefficients of the GL theory, Eq. (3.4), as

$$r = \frac{N(0)}{2}\left(\frac{1}{|F_l^a|} - \frac{1}{2} \right),$$

$$v_1 = \frac{N(0)}{32}\left\{ \left[\frac{N'(0)}{N(0)} \right]^2 - \frac{N''(0)}{2N(0)} \right\} = (1 - a - 2a^2 + 3b)\frac{N(0)}{32 v_F^2 k_F^2},$$

$$v_2 = \frac{N''(0)}{48} = (-a + 2a^2 - b)\frac{N(0)}{8 v_F^2 k_F^2}, \quad (4.12)$$

where $v_{1,2}$ do not depend on the value of l at the mean-field level. $N'(0)$ and $N''(0)$ are the first- and second-order derivatives of density of states at the Fermi energy E_f, respectively. They are defined as

$$N'(0) = \left. \frac{dN}{d\epsilon} \right|_{\epsilon = E_F} = (1 - 2a)\frac{N(0)}{v_F k_F},$$

$$N''(0) = \left. \frac{d^2 N}{d\epsilon^2} \right|_{\epsilon = E_F} = 6(-a + 2a^2 - b)\frac{N(0)}{v_F^2 k_F^2}. \quad (4.13)$$

Both of them only depend on the nonlinear dispersion relation up to the cubic order as kept in Eq. (2.5).

It is worth it to stress that the coefficients of Eq. (4.12) were calculated (within this mean-field theory) at *fixed density*. Similar coefficients were obtained in the spinless system analyzed in Ref. 4 at fixed chemical potential. There is a subtle difference between these two settings in the behavior of the quartic terms. At fixed chemical potential, the sign of b, the coefficient of the cubic term in the free fermion dispersion relation, is crucial for the nematic phase to be stable. However, as can be seen in Eq. (4.12), the sign of the coefficient of the quartic term v_1 is determined by several effects:

the coefficients a and b, and that of an extra (additive) contribution, which originates from the curvature of the Fermi surface and hence scales as $N(0)/k_F^2$. It has been noted in Refs. 23, 47, and 48 that the nematic instability for lattice systems may be a continuous quantum phase transition or a first-order transition, in which case it involves a change in the topology of the Fermi surface. As shown above, this dichotomy is the result of the interplay of the single-particle dispersion and effects due to the curvature of the Fermi surface. The same considerations apply to the coefficients that we will present in the following subsection.

The ground-state spin configuration in the β phase exhibits a vortex structure with winding number $w = l$ in momentum space. The case of $w = 2$ is depicted in Fig. 3(a). Interestingly, in the case of $l = 3$, after setting $\vec{d} = (\cos(3\theta + \pi/2), \sin(3\theta + \pi/2), 0)$, the effective single-particle Hamiltonian becomes

$$H_{\mathrm{MF}}(k) = \epsilon(k) + \bar{n}[-\sin(3\theta_k)\sigma_x + \cos(3\theta_k)\sigma_y]. \quad (4.14)$$

This single-particle Hamiltonian has the same form as that of the heavy-hole band of the two-dimensional n-doped GaAs system,[49,50] which results from SO coupling.

Now we discuss the general configuration of the d vector in the β phase in the F_l^a channel. $\vec{n}_1$ and $\vec{n}_2$ can be any two orthogonal unit vectors on the S^2 sphere. The plane spanned by $\vec{n}_{1,2}$ intersects the S^2 sphere at any large circle, as depicted in Fig. 4, which can always be obtained by performing a suitable SO(3) rotation from the large circle in the xy plane. The spin configuration around the Fermi surface maps to this large circle with the winding number of l. Furthermore, the configurations of winding number $\pm l$ are equivalent to each other up to rotation of π around a diameter of the large circle. For example, the case of $w = -2$ is depicted in Fig. 3(b), which can be obtained from that of $w = 2$ by performing such a rotation around the $\hat{x}$ axis. Similarly, with the $SO_S(3)$ symmetry in the spin space, the configurations with $w = \pm l$ are topologically equivalent to each other. However, if the $SO_S(3)$ symmetry is reduced to $SO_S(2)$ because of the existence of an explicit easy-plane magnetic anisotropy (which is an effect of SO interactions at the single-particle level), or by
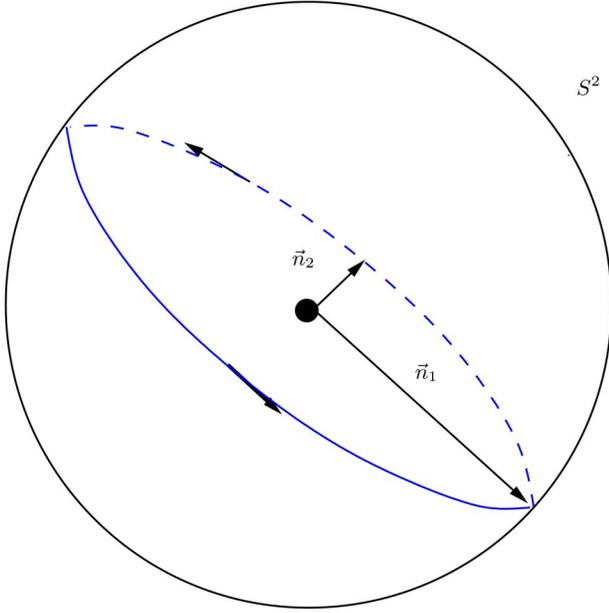
FIG. 4. (Color online) The spin configurations on both Fermi surfaces in the β phase (F_l^a channel) map to a large circle on an S^2 sphere with the winding number l.

an external magnetic field $\vec{B}$, then the two configurations with $w = \pm l$ belong to two distinct topological sectors.

C. 3D instabilities of the *p*-wave spin-triplet channel

The mean-field theory for the Pomeranchuk instability in the F_1^a channel has been studied in Ref. 30. To make the paper self-contained, here we summarize the main results.

In the α phase, taking the special case $n^{\mu a} = \bar{n} \delta_{\mu z} \delta_{az}$, the mean-field Hamiltonian reads

$$H_{3D,\alpha} = \int \frac{d^3 k}{(2\pi)^3} \psi^\dagger(\vec{k})[\epsilon(\vec{k}) - \mu - \bar{n}\sigma_z \cos\theta_k]\psi(\vec{k}),$$

$$(4.15)$$

where θ is the angle between $\vec{k}$ and the z axis. The Fermi surfaces for the two spin components are distorted in the opposite way as

$$\frac{\Delta k_{F\uparrow,\downarrow}(\theta)}{k_F} = \frac{1}{3}(1-a)x^2 \pm \left[x + \frac{2}{3}a(1-a)^3 x^3 \right] \cos\theta$$
$$- ax^2 \cos^2\theta \pm (2a^2 - b)x^3 \cos^3\theta + O(x^4).$$

$$(4.16)$$

In the β phase, rotational symmetry is preserved and a SO interaction is dynamically generated. With the ansatz $n^{\mu a} = \bar{n}\delta_{\mu a}$, the MF Hamiltonian reduces to

$$H_{3D,\beta} = \sum_k \psi^\dagger(k)[\epsilon(k) - \mu - \bar{n}\vec{\sigma} \cdot \hat{k}]\psi(k). \quad (4.17)$$

The single-particle states can be classified according to the eigenvalues ± 1 of the helicity operator $\vec{\sigma} \cdot \hat{k}$, with dispersion relations $\xi^B(k)_{\uparrow,\downarrow} = \epsilon(k) - \mu \pm \bar{n}$. The Fermi surfaces split into

two parts, but still keep the round shape for two helicity bands with

$$\frac{\Delta k_{F\uparrow,\downarrow}}{k_F} = \pm x - x^2 \pm (2a-b)x^3 + O(x^4). \quad (4.18)$$

The β phase is essentially isotropic. The orbital angular momentum $\vec{L}$ and spin $\vec{S}$ are no longer separately conserved, but the total angular momentum $\vec{J} = \vec{L} + \vec{S} = 0$ remains conserved instead. For the general case of $n_{\mu a} = \bar{n}D_{\mu a}$, it is equivalent to a redefinition of spin operators as $S'_\mu = S_\nu D_{\nu a}\delta_{a\mu}$; thus Fermi-surface distortions remain isotropic and $\vec{J}' = \vec{L} + \vec{S}'$ is conserved.

From the above mean-field theory, we can calculate the coefficients in Eq. (3.11) as

$$r' = \frac{N(0)}{2}\left(\frac{1}{|F_1^a|} - \frac{1}{3} \right),$$

$$v_1' = \frac{N(0)}{24}\left\{ \frac{1}{3}\left[\frac{N'(0)}{N(0)} \right]^2 - \frac{N''(0)}{5N(0)} \right\}$$
$$= \frac{N(0)}{180 v_F^2 k_F^2}(7 - 2a - 8a^2 + 9b),$$

$$v_2' = \frac{N_2(0)}{90} = \frac{N(0)}{45 v_F^2 k_F^2}(1 - 6a + 6a^2 - 3b), \quad (4.19)$$

where

$$N'(0) = \left. \frac{dN}{d\epsilon} \right|_{\epsilon = E_F} = \frac{2 - 2a}{v_F k_F}N(0),$$

$$N''(0) = \left. \frac{d^2 N}{d\epsilon^2} \right|_{\epsilon = E_F} = \frac{2(1 - 6a + 6a^2 - 3b)}{v_F^2 k_F^2}N(0).$$

$$(4.20)$$

Once again, the caveats of the previous subsection on the sign of the coefficients of the quartic terms apply here too.

V. GOLDSTONE MANIFOLDS AND TOPOLOGICAL DEFECTS

In this section, we will discuss the topology of the broken symmetry α and β phases and their associated Goldstone manifolds in two and three dimensions. We will also discuss and classify their topological defects. We should warn the reader that the analysis we present here is based only on the static properties of the broken-symmetry phases and ignores potentially important physical effects due to the fact that in these systems the fermions remain gapless (although quite anomalous). In contrast, in anisotropic superconductors the fermion spectrum is gapped (up to possibly a set of measure zero of nodal points of the Fermi surface). The physics of these effects will not be discussed here.

A. Topology of the α phases

1. 2D α phases

For the 2D α phases, for which we can set $\langle n^{\mu a} \rangle = \bar{n} \delta_{\mu z} \delta_{a1}$, the system is invariant under $SO_S(2)$ rotation in the spin channel, the $\mathbb{Z}_l$ rotation with the angle of $2\pi/l$ in the orbital channel, and a $\mathbb{Z}_2$ rotation with the angle of π around the x axis in the spin channel combined with an orbital rotation at the angle of π/l. Thus, the Goldstone manifold is

$$[SO_L(2) \otimes SO_S(3)]/[SO_S(2) \ltimes \mathbb{Z}_2 \otimes \mathbb{Z}_l]$$
$$= [SO_L(2)/\mathbb{Z}_l] \otimes [S^2/\mathbb{Z}_2], \qquad (5.1)$$

giving rise to three Goldstone modes: one describes the oscillation of the Fermi surface, while the other two describe the spin precession. Their dispersion relation will be calculated in Sec. VII A.

Due to the $\mathbb{Z}_2$ structure of the combined spin-orbit rotation, the vortices in the 2D α phase can be divided into two classes. The first class is the $1/l$ vortices purely in the orbital channel without distortions in the spin channel. This class of vortices has the same structure as that in the Pomeranchuk instabilities in the density channel dubbed the integer quantum vortex. On the other hand, another class of vortices as combined spin-orbital defects exists. This class of vortices bears a structure similar to that of the half-quantum vortex (HQV) in a superfluid with internal spin degrees of freedom.[51–53] An example vortex at $l=1$ of this class is depicted in Fig. 5, where the π disclination in the orbit channel is offset by the rotation of π around the x axis in the spin channel. To describe the vortex configuration for the case of the p-wave channel, we set up a local reference frame in spin space and assume that the electron spin is either parallel or antiparallel to the z axis of this frame, at a point $\vec{x}$ in real space. Let $\phi=0$ be the angular polar coordinate of $\vec{x}$ with respect to the core of the vortex. As we trace a path in real space around the vortex, the frame in spin space rotates so that the spin flips its direction from up to down (or vice versa) as we rotate by an angle of π. (In the d-wave channel, the vortex involves a rotation by $\pi/2$.) Such behavior is a condensed-matter example of the Alice-string behavior in the high-energy physics.[54,55] Another interesting behavior of HQV is that a pair of half-quantum vortex and antivortex can carry a spin quantum number. This is a global example of the Cheshire charge in the gauge theory.[51,53] The electron can exchange spin with the Cheshire charged HQV pairs when it passes in between the HQV pairs.

Due to the $SO(2)_L \times SO_S(2)$ symmetry in the Hamiltonian, the fluctuations in the orbital channel are less severe than those in the spin channel. In the ground state, the spin stiffness should be softer than that in the orbital channel. As a result, an integer-valued vortex should be energetically favorable to fractionalize into a pair of HQV. However, at finite temperatures, in the absence of magnetic anisotropy (an effect that is ultimately due to spin-orbit effects at the atomic level) the spin channel is disordered with exponentially decaying correlation functions, and thus without long-range order in the spin channel. However, the orbital channel still

exhibits the Kosterlitz-Thouless behavior at two-dimensions, where the low-energy vortex configurations should be of HQV.

2. 3D α phases

Similarly, the Goldstone manifold in the 3D α phase for $l=1$ can be written as

$$[SO_L(3) \otimes SO_S(3)]/[SO_L(2) \otimes SO_S(2) \ltimes \mathbb{Z}_2] = [S_L^2 \otimes S_S^2]/\mathbb{Z}_2, \qquad (5.2)$$

where again the $\mathbb{Z}_2$ operation is a combined spin-orbit rotation at the angle of π to reverse the spin polarization and orbital distortion simultaneously. This Goldstone mode manifold gives rise to two Goldstone modes in the density channel responsible for the oscillations of the distorted Fermi surfaces and another two Goldstone modes for the spin precessions. The fundamental homotopy group of Eq. (5.2) reads $\pi_1[S_L^2 \otimes S_S^2]/\mathbb{Z}_2 = \mathbb{Z}_2$. This means that the π disclination exists as a stable topological line defect. On the other hand, for the point defect in 3D space, the second homotopy group of Eq. (5.2) reads $\pi_2([S_L^2 \otimes S_S^2]/\mathbb{Z}_2) = \mathbb{Z} \otimes \mathbb{Z}$. This means that both the orbit and the spin channels can exhibit monopole (or hedgehog) structures characterized by a pair of winding numbers (m, n). As a result of the $\mathbb{Z}_2$ symmetry, (m, n) denotes the same monopoles as that of $(-m, -n)$.

B. Topology of the β phases

In the 2D β phase with $l=1$ and $w=1$ in the xy plane, the ground state is rotationally invariant; thus, $L_z + \sigma_z/2$ is still conserved. Generally speaking, the 2D β phases with the momentum space winding number w is invariant under the combined rotation generated by $L_z + w\sigma_z/2$. The corresponding Goldstone manifold is

$$[SO_L(2) \otimes SO_S(3)]/SO_{L+S}(2) = SO(3). \qquad (5.3)$$

Three Goldstone modes exist as relative spin-orbit rotations around the x, y, and z axes on the mean-field ground state. Similarly, for the 3D β phase with $l=1$, the Goldstone mode manifold is

$$[SO_L(3) \otimes SO_S(3)]/SO(3)_{L+S} = SO(3), \qquad (5.4)$$

with three branches of Goldstone modes. The dispersion relation of these Goldstone modes will be calculated in Sec. VIII. The vortexlike point defect in two dimensions and the line defect in three dimensions are determined by the fundamental homotopy group $\pi_1(SO(3)) = \mathbb{Z}_2$. On the other hand, the second homotopy group $\pi_2(SO(3)) = 0$; thus, as usual, no topologically stable point defect exists in three dimensions.

VI. THE RPA ANALYSIS IN THE CRITICAL REGION AT ZERO TEMPERATURE

In this section, we study the collective modes in the Landau FL phase as the Pomeranchuk quantum critical point is approached, $0 > F_l^a > -2$ in two dimensions and $0 > F_l^a > -3$ in three dimensions. These collective modes are the high partial-wave channel counterparts of the paramagnon modes
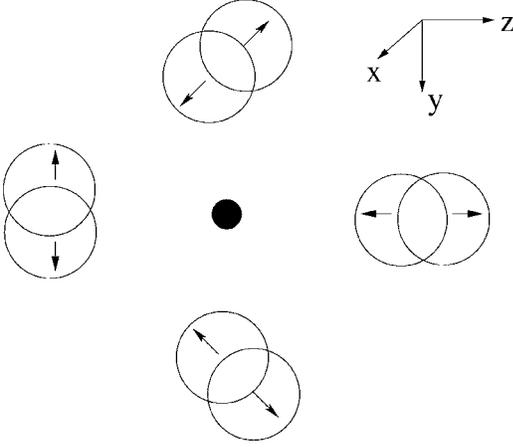
FIG. 5. The half-quantum vortex with the combined spin-orbit distortion for the α phase at $l=1$. The triad denotes the direction in the spin space.

in the ^{3}He system. The picture of collective modes in the p-wave channel at two dimensions is depicted in Fig. 6.

For this analysis, it is more convenient to employ the path integral formalism and perform the Hubbard-Stratonovich transformation to decouple the 4-fermion interaction term of the Hamiltonian presented in Eq. (2.4). After integrating out the fermionic fields, we arrive at the effective action,

$$S_{\text{eff}}(\vec{n}_b) = -\frac{1}{2}\int_0^\beta d\tau \int d\vec{r}d\vec{r}' (f_1^a)^{-1}(\vec{r}-\vec{r}')\vec{n}_b(\vec{r}) \cdot \vec{n}_b(\vec{r}')$$
$$+ \text{tr} \ln\left[\frac{\partial}{\partial\tau} + \epsilon(\vec{\nabla}) - \vec{n}_b(\vec{r}) \cdot \vec{\sigma}g_{l,b}(-i\vec{\nabla})\right]. \quad (6.1)$$

In the normal FL state, we set $\bar{n}=0$, the fluctuations at the quadratic level are given by the effective action,

$$S_{\text{FL}}^{(2)}(n) = \frac{1}{2V\beta}\sum_{\vec{q},i\omega_n} n^{\mu a}(\vec{q},i\omega_n)L_{\mu a,vb}^{(\text{FL})}(\vec{q},i\omega_n)n^{vb}(-\vec{q},-i\omega_n),$$
$$(6.2)$$

where we have introduced the fluctuation kernel $L_{\mu a,vb}(\vec{q},i\omega_n)$, which is given by

$$L_{\mu a,vb}^{(\text{FL})}(\vec{q},i\omega_n) = -(f_1^a)^{-1}(q)\delta_{\mu\nu}\delta_{ab} + \langle Q^{\mu,a}(\vec{q},i\omega_n)$$
$$\times Q^{v,b}(-\vec{q},-i\omega_n)\rangle_{\text{FL}}, \quad (6.3)$$

and

$$\langle Q^{\mu,a}(\vec{q},i\omega_n)Q^{v,b}(-\vec{q},-i\omega_n)\rangle_{\text{FL}}$$
$$= \frac{1}{V\beta}\sum_{\vec{k},i\omega_{n'}} \text{tr}[G^{(\text{FL})}(\vec{k}+\vec{q},i\omega_{n'}+i\omega_n)\sigma^\mu g_a(\hat{k})$$
$$\times G^{(\text{FL})}(\vec{k},i\omega_{n'})\sigma^v g_b(\hat{k})] \quad (6.4)$$

is the correlation function of the $Q^{\mu,a}$ operators, defined in Eq. (2.3), in the FL phase (i.e., a fermion bubble). Here,

$$G^{(\text{FL})}(\vec{k},i\omega_n) = \frac{1}{i\omega_n - \epsilon(\vec{k})} \quad (6.5)$$

is the fermion Green's function in the FL phase, and it is diagonal in spin space.

After performing the Matsubara frequency summation, we find that the fluctuation kernel in the FL phase is given by the expression,

$$L_{\mu a,vb}^{(\text{FL})}(q,\omega) = -(f_l^a)^{-1}(q)\delta_{\mu\nu}\delta_{ab}$$
$$+ 2\delta_{\mu\nu}\int \frac{d^dk}{(2\pi)^d}\frac{n_f(\epsilon_{k-q/2}) - n_f(\epsilon_{k+q/2})}{\omega + i\eta + \epsilon_{k-q/2} - \epsilon_{k+q/2}}A_{ab},$$
$$(6.6)$$

where we have performed an analytic continuation to real frequency ω, and A_{ab} is an angular form factor to be defined below.

A. Two dimensions

In two dimensions, without loss of generality, we can choose the direction of $\vec{q}$ along the x axis where the azimuthal angle $\theta=0$. The fluctuation kernels are given by

$$L_{\mu a,vb}^{(\text{FL})}(q,w) = \delta_{ab}\delta_{\mu\nu}\left[\kappa q^2 + \delta\right.$$
$$\left. + \frac{N(0)}{2}\int_{-1}^1 \frac{d\theta}{2\pi}\frac{s}{s + i\eta - \cos\theta}A^{ab}\delta_{ab}\right],$$

$$s = \omega/(v_Fq), \quad \delta = N(0)\left(\frac{1}{|F_1^a(0)|} - \frac{1}{2}\right) > 0, \quad (6.7)$$

where, as before, $\mu,\nu=x,y,z$ are the components of the spin vector, and $a,b=1,2$ are the two orbital components. The diagonal components of the angular form factors are $A^{aa} = (\cos^2 l\theta, \sin^2 l\theta)$. For $s < 1$, the angular integral can be performed to yield

$$\int_0^{2\pi} \frac{d\theta}{2\pi}\frac{s}{s + i\eta - \cos\theta}\begin{pmatrix}\cos^2 l\theta \\ \sin^2 l\theta\end{pmatrix}$$
$$= \frac{s}{2i\sqrt{1-s^2}}[1 \pm (s - i\sqrt{1-s^2})^{2l}]. \quad (6.8)$$

For $s \ll 1$, we can expand the above integral and find, for l odd,

$$L_{\mu a,vb}^{(\text{FL})}(q,\omega) = \delta_{ab}\delta_{\mu\nu}[\kappa q^2 + \delta + N(0)]$$
$$\times \begin{cases} -ls^2 - il^2s^3 & \text{for } a=1 \\ ls^2 - is & \text{for } a=2. \end{cases} \quad (6.9)$$

Here, since we have chosen $\vec{q}$ along the x axis, the component $a=1$ denotes the longitudinal component (parallel to the direction of propagation $\vec{q}$) and $a=2$ is the transverse component. Similarly, for l even, we get

$$L_{\mu a,vb}^{(\text{FL})}(q,\omega) = \delta_{ab}\delta_{\mu\nu}[\kappa q^2 + \delta + N(0)]$$
$$\times \begin{cases} ls^2 - is & \text{for } a=1 \\ -ls^2 - il^2s^3 & \text{for } a=2. \end{cases} \quad (6.10)$$

A: transverse modes
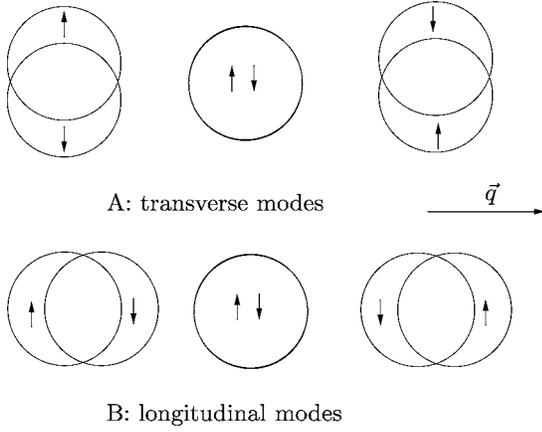
$\vec{q}$

B: longitudinal modes

FIG. 6. The p-wave counterpart of paramagnon modes in 2D. Taking into account the spin degrees of freedom, there are three (six) transverse triplet modes in 2D (3D) and three longitudinal modes, respectively.

When l is odd, the transverse modes are overdamped and the longitudinal modes are underdamped. For example, in the case of $l=1$, the dispersion relation at the critical point $\delta \to 0^+$ can be solved as

$$\omega_2(q) = -i\frac{\kappa v_F q^3}{N(0)}, \qquad (6.11)$$

for the transverse mode, and

$$\omega_1(q) = \sqrt{\frac{\kappa}{N(0)}} v_F q^2 - i\frac{\kappa}{2N(0)} v_F q^3, \qquad (6.12)$$

for the longitudinal mode. In contrast, when l is even, such as the instability in the F_2^s channel, the transverse part is underdamped and the longitudinal part is overdamped.[4] The difference is due to the different behaviors of the angular form factors for l even and l odd, respectively.

In both cases, just as it was found in Ref. 4, the dynamic critical exponent is $z=3$. By the power counting, the bare scaling dimension of the quartic terms in the GL free energy, with effective coupling constants v_1 and v_2, is $(d+z)-4$, where d is the spatial dimension, while the scaling dimension of the γ_2 term linear in spatial derivatives is $(d+z)/2-2$. All of these operators are irrelevant at zero temperature in two and three dimensions. Thus, the critical theory is Gaussian, at least in the perturbation theory. However, it is possible that the above naive scaling dimensional analysis may break down at the quantum critical point. Various authors have found nonanalytic corrections to Fermi liquid quantities at the ferromagnetic quantum critical point.[56] This may also occur here as well. We will defer a later research for the study of these effects. At finite temperatures, the critical region turns out to be non-Gaussian.[45] Both the terms whose couplings are γ_2 and $v_{1,2}$ now become relevant. The relevance of the γ_2 term does not appear in the usual ferromagnetic phase transitions,[57] and we will also defer the discussion of this effect to a future publication.

B. Three dimensions

In three dimensions, we can choose the z axis along the direction of $\vec{q}$. The diagonal part of the angular form factors is now $A^{aa}=(\sin^2 \theta/2, \sin^2 \theta/2, \cos^2 \theta)$. Assuming that $|q| \ll k_F$, the fluctuation kernel can be approximated as

$$L_{\mu a,vb}^{(\mathrm{FL})}(q,\omega) = \delta_{ab}\delta_{\mu v}\left[\kappa q^2 + \delta \right.$$
$$\left. + \frac{N(0)}{2}\int_{-1}^{1} d\cos \theta \frac{s}{s+i\eta-\cos \theta}A^{aa} \right],$$

$$s = \omega/(v_F q), \quad \delta = N(0)\left(\frac{1}{|F_1^a(0)|} - \frac{1}{3}\right) > 0, \quad (6.13)$$

where $\mu, v = x, y, z$ are once again the three components of the spin vector. For the $l=1$ (p-wave) case, $a,b=1,2,3$ are the three orbital components. Using the formula

$$\ln\left(\frac{s+1}{s+i\eta-1}\right) = \ln\left|\frac{s+1}{s-1}\right| - i\pi\Theta(s<1), \quad (6.14)$$

we arrive at

$$L_{\mu a,vb}^{(\mathrm{FL})}(q,\omega) = \delta_{ab}\delta_{\mu v}(\kappa q^2 + \delta)$$
$$+ \delta_{ab}\delta_{\mu v}\begin{cases} N(0)\left(s^2 - i\frac{\pi}{4}s\right) & \text{for } a=1,2 \\ -N(0)\left(s^2 + i\frac{\pi}{2}s^3\right) & \text{for } a=3, \end{cases}$$

$$(6.15)$$

where only the leading-order contribution to the real and imaginary parts is kept. The dispersion relation at the critical point $\delta \to 0^+$ can be solved as

$$\omega_{1,2}(q) = -i\frac{4v_F}{\pi}\frac{\kappa q^3}{N(0)}, \qquad (6.16)$$

for the transverse modes, and

$$\omega_3(q) = \sqrt{\frac{\kappa}{N(0)}} v_F q^2 - i\frac{\pi}{4}\frac{\kappa}{N(0)} v_F q^3, \qquad (6.17)$$

for the longitudinal mode. Similar to the case in two dimensions, the longitudinal channel is weakly damped and the other two transverse channels are overdamped. Again the dynamic critical exponent $z=3$; thus, naively the critical theory is Gaussian at zero temperature.

VII. GOLDSTONE MODES IN THE α PHASE

At the RPA level, the Gaussian fluctuations around the mean-field saddle point of the α phase are described by an effective action of the form,

$$S_\alpha^{(2)}(n) = \frac{1}{2V\beta}\sum_{\vec{q},i\omega_n} \delta n^{\mu a}L_{\mu a,vb}^{(\alpha)}(\vec{q},i\omega_n)\delta n^{vb}. \qquad (7.1)$$

The fluctuation kernel in the α phase is

$$L_{\mu a,vb}^{(\alpha)}(\vec{q},i\omega_n) = -(f_1^a)^{-1}(q)\,\delta_{\mu v}\delta_{ab} + \langle Q^{\mu,a}(\vec{q},i\omega_n)$$
$$\times Q^{v,b}(-\vec{q},-i\omega_n)\rangle_\alpha, \qquad (7.2)$$

where

$$\langle Q^{\mu,a}(\vec{q},i\omega_n)Q^{v,b}(-\vec{q},-i\omega_n)\rangle_\alpha$$
$$= \frac{1}{V\beta}\sum_{\vec{k},i\omega_{n'}} \text{tr}[G^{(\alpha)}(\bar{n},k+q,i\omega_{n'}+i\omega_n)\sigma^\mu g_{l,a}(\hat{k})$$
$$\times G^{(\alpha)}(\bar{n},k,i\omega_{n'})\sigma^v g_{l,b}(\hat{k})] \qquad (7.3)$$

is the correlator of the operators $Q^{\mu a}$ in the mean-field theory ground state of the α phase (again a fermion bubble). Here, $G^{(\alpha)}(\bar{n},\vec{k},i\omega_n)$ is the fermion propagator in the α phase with an expectation value of the (nematic-spin-nematic for the $l = 2$ case) order parameter equal to $\bar{n}$,

$$G^{(\alpha)}(\bar{n},\vec{k},i\omega_n) = [i\omega_n - \varepsilon_\alpha(\vec{k},\bar{n})]^{-1}, \qquad (7.4)$$

where

$$\varepsilon_\alpha(\vec{k},\bar{n}) = \varepsilon(\vec{k}) - \langle\vec{n}_b\rangle_\alpha \cdot \vec{\sigma} g_{l,b}(\hat{k}),$$

$$g_{l,1}(\vec{k}) = \cos l\theta_{\vec{k}}, \quad g_{l,2}(\vec{k}) = \sin l\theta_{\vec{k}} \qquad (7.5)$$

is the fermion dispersion, a matrix in spin space, and $\langle\vec{n}_b\rangle_\alpha = \bar{n}\hat{z}\delta_{b,1}$ is the mean-field expectation value of the order parameter in the α phase.

Since in the α phase there are spontaneously broken continuous symmetries, in both two and three dimensions, the collective modes will consist of gapped longitudinal modes, i.e., along the direction of the condensate, and gapless, Goldstone, modes transverse to the direction of spontaneous symmetry breaking, both in the density and spin channels. We will discuss the Goldstone modes in the β phase in the next section.

We next comment on the stability of the α phase in the *p*-wave channel. The GL energies [Eqs. (3.5) and (3.12)] contain a cubic term linear in derivatives. In the ordered state, it might induce a linear derivative coupling between the massless Goldstone mode at the quadratic level through the condensate longitudinal mode, thus leading to a Lifshitz instability in the ground state. As we will show, this indeed occurs in the *p*-wave β phase. However, we will see that in the α phase, the spin (density) channel Goldstone modes have the same orbital (spin) indices as those of the longitudinal mode; thus, they cannot be coupled by Eqs. (3.5) and (3.12). Instead, the Goldstone modes couple to other gapped modes at the quadratic level through linear derivative terms, which do not lead to instability at weak coupling, but can renormalize the stiffness of the Goldstone modes.

A. 2D α phases

We consider the 2D α phases assuming the order-parameter configuration as $\langle n_{\mu b}\rangle = \bar{n}\delta_{\mu z}\delta_{b1}$. The order parameter is thus the operator $n_{z,1}$ of Eqs. (2.1) and (2.2). As studied in Sec. IV A, the Goldstone mode manifold $S^2 \times SO_L(2)$ results in one branch of Goldstone mode in the

density channel and two branches of Goldstone modes in the spin channel. The fluctuation kernel of the α phases, $L_{\mu a,vb}^{(\alpha)}$, is a 6×6 matrix. Its eigenvalues will thus yield six collective modes of which three are the above-mentioned Goldstone modes. The other three modes are gapped, and are associated with the structure of the order parameter in the α phases. In the low-frequency regime, $\omega \ll \bar{n}$, we can neglect the mixing between the Goldstone modes and other gapped modes.

The density channel Goldstone mode is associated with the field $n_{z,2}$, conjugate to the bilinear fermion operator $Q_{z,2}$, which is longitudinal in the spin sector and transverse in the charge sector,

$$Q_{z2}(\vec{r}) = \psi_\alpha^\dagger(\vec{r})[\sigma_{z,\alpha\beta}(-i\nabla_y)]\psi_\beta(\vec{r}), \qquad (7.6)$$

and describes the Fermi-surface oscillation in the 2-direction while keeping the spin configuration unchanged. On the other hand, the spin channel Goldstone modes $n_{sp,x\pm iy}$, conjugate to the fermion bilinears $Q_{x\pm iy,1} = (Q_{x,1}\pm iQ_{y,1})/2$, describe spin oscillations while keeping the Fermi surface unchanged.

1. Density channel Goldstone mode

The density channel Goldstone field $n_{z,2}$ behaves similarly to its counterpart in the density channel Pomeranchuk instability.[4] The same approximation as in Ref. 4 can be used to deal with the anisotropic Fermi surface, i.e., keeping the anisotropy effect in the static part of the correlation function, but ignoring it in the dynamic part. This approximation is valid at small values of the order parameter, i.e., $x = \bar{n}/(v_F k_F) \ll 1$, where $\bar{n} = \langle n_{z,1}\rangle$. We define the propagation wave vector $\vec{q}$ with the azimuthal angle ϕ as depicted in Fig. 7 for the $l=1$ case.

The effective fluctuation kernel for the charge channel Goldstone mode, which we label by fs, reduces to

$$L_{fs}^{(\alpha)}(\vec{q},\omega) = \kappa q^2 - N(0)$$
$$\times \begin{cases} is\sin^2(l\phi) - ls^2\cos(2l\phi) & (l \text{ even}) \\ is\cos^2(l\phi) + ls^2\cos(2l\phi) & (l \text{ odd}), \end{cases}$$
$$(7.7)$$

where $s = \omega/v_F q$. Similar to the results Ref. 4, this Goldstone mode corresponding to Fermi-surface oscillation is over-damped almost on the entire Fermi surface except on a set of directions of measure zero: for l even, the charge channel Goldstone mode is underdamped in the directions $\phi = n\pi/l$, $n = 0, 1, \ldots, l$, which are just the symmetry axes of the Fermi surface; for l odd, it is underdamped instead in the directions $\phi = \pi(n+1/2)/l$, and in this case the Goldstone mode is maximally damped along the symmetry axes.

2. Spin channel Goldstone modes

On the other hand, the spin channel Goldstone fields $n_{x\pm iy,1}$ behave very differently. They only involve "interband transitions," leading instead to a fluctuation kernel of the form,

$$L_{x+iy,1}(\vec{q}, \omega) = \kappa q^2 + \frac{1}{|f_1^a|} + 2 \int \frac{d^2k}{(2\pi)^2} \cos^2(l\theta_k)$$

$$\times \frac{n_f[\xi_\downarrow(\vec{k} - \vec{q}/2)] - n_f[\xi_\uparrow(\vec{k} + \vec{q}/2)]}{\omega + i\eta + \xi_\downarrow(\vec{k} - \vec{q}/2) - \xi_\uparrow(\vec{k} + \vec{q}/2)},$$

$$(7.8)$$

where $\xi_{1,2}(k) = \epsilon(\vec{k}) - \mu \mp \bar{n} \cos(l\theta_k)$. They satisfy the relation

$$L_{x-iy,1}(\vec{q}, \omega) = L_{x+iy,1}(-\vec{q}, -\omega). \qquad (7.9)$$

A detailed calculation, presented in Appendix B, shows that for $\omega/\bar{n}, v_F q/\bar{n} \ll 1$, the kernel $L_{x\pm iy,1}$ reads

$$L_{x\pm iy,1}(\vec{q}, \omega) = \kappa q^2 - \frac{N_0}{2|F_l^a|} \frac{\omega^2}{\bar{n}^2}, \qquad (7.10)$$

which gives rise to a linear and undamped spectrum:

$$\omega_{x\pm iy,1}(\vec{q}) = \sqrt{\frac{2\kappa |F_l^a|}{N(0)}} \bar{n} |\vec{q}|. \qquad (7.11)$$

Equation (7.11) has to two important features (due to the interband transition): the isotropy of dispersion relation at $\omega/\bar{n}, v_F q/\bar{n} \ll 1$ in spite of the anisotropic Fermi surfaces, and the underdamping of the Goldstone modes. The contribution to the integral comes from the region around Fermi surfaces with the width of about $2\bar{n} \cos(l\theta_k)/v_F$. The dependence of the integral on $\vec{q}$ can be neglected at $v_F q/\bar{n} \ll 1$ because a small $\vec{q}$ changes the integration area weakly, and it thus matters only for high-order corrections in $\vec{q}$. The contribution to damping comes from the region where two bands become nearly degenerate, i.e., $\cos(l\theta_k) \approx 0$. However, the angular form factor also takes the form of $\cos(l\theta_k)$, which tends to suppress damping. As $v_F q$ becomes comparable to $\bar{n}$, the anisotropy and damping effects become more important.

The linear dispersion relation for the spin channel Goldstone modes at $v_F q/\bar{n} \ll 1$ holds regardless of whether l is odd or even. This fact is closely related TR and parity symmetry properties of the order parameter $n^{\mu a}$. For l odd, $n^{\mu a}$ is *even* under TR transformation, and hence terms linear in time derivatives cannot appear in the effective action. On the other hand, for l even, although $n^{\mu a}$ is *odd* under TR, in two dimensions, we can still define the combined transformation T' as

$$T' = TR(\pi/l), \qquad (7.12)$$

under which $n^{\mu a}$ is even. Here, $R(\pi/l)$ is a real-space rotation by an angle of π/l. Thus, also in this case, terms, which are linear in time derivative are not allowed in the effective action. In contrast, for the case of a ferromagnet at $l=0$, TR symmetry is broken, and no other symmetry exists to form a combined operation T' that will leave the system invariant. As a result, terms linear in time derivatives appear in the effective action of a ferromagnet. The same arguments apply for phases with mixed ferromagnetic and spin-nematic order (and its generalizations). Furthermore, in the presence of time-reversal-violating terms, the two transverse components of spin fluctuation become conjugate to each other as in the presence of ferromagnetic long-range order. In this case, only
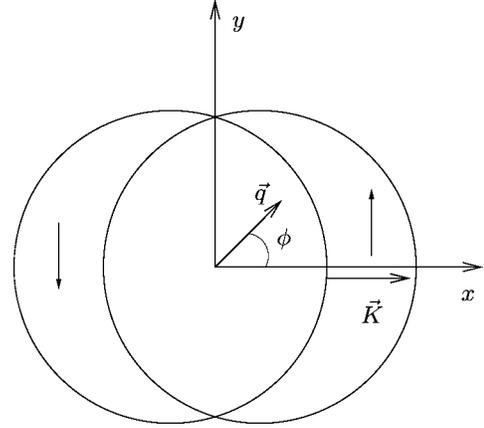

FIG. 7. The azimuthal angle ϕ for the propagation wave vector $\vec{q}$ for the Goldstone modes in the 2D alpha phase. The spin-down and -up Fermi surfaces can overlap each other by a shift at the wave vector $\vec{K} = 2\bar{n}/v_F$.

one branch of spin-wave Goldstone mode exists with a quadratic dispersion relation $\omega_{FM} \propto q^2$.

3. Spin-wave spectra

We assume that the F_0^a channel is off-critical; thus, in the normal state no well-defined spin-wave modes exist. However, in the α phase the spin channel Goldstone modes carry spin, and thus induce a well-defined pole in the spin-wave spectrum. This can be understood from the commutation relation between spin modes and the spin channel Goldstone modes

$$[S_x \pm iS_y, Q_{x\mp iy,1}] = \pm 2Q_{z,1}. \qquad (7.13)$$

In the α phase where Q_{z1} obtains a nonvanish expectation value, then these two channels become conjugate. As a result, the spin wave gains a sharp resonance which should appear in the neutron-scattering experiment. In contrast, in the normal state, the coupling between this two modes is negligible, and thus the resonance disappears. A similar physics occurs in the SO(5) theory for the explanation of π resonance in the underdoped high T_c cuprates.[58]

The effective coupling constant, which mixes the S_x+iS_y and $Q_{x-iy,1}$ operators is a bubble diagram, which can be calculated as

$$\chi_s^0(\vec{q}, \omega) = -N(0) \frac{\omega}{\bar{n}}. \qquad (7.14)$$

This bubble is dressed by the interaction in the F_l^a channel. The resonant part of the spin correlation function (i.e., the contribution of the collective mode pole) becomes

$$\chi_s(\vec{q}, \omega) = \langle S_+(\vec{q}, \omega) S_-(-\vec{q}, -\omega) \rangle$$

$$= \frac{|\chi_s^0(\vec{q}, \omega)|^2}{L_{x+iy,1}(\vec{q}, \omega)}$$

$$= \frac{N(0) \dfrac{\omega^2}{\bar{n}^2}}{\dfrac{\kappa q^2}{N(0)} - \dfrac{2}{|F_l^a|} \dfrac{\omega^2}{\bar{n}^2} - i\delta}. \qquad (7.15)$$

For fixed but small $\vec{q}$, the spectral function exhibits a δ-function peak at the dispersion of the collective mode,

$$\text{Im } \chi_s(\vec{q},\omega) = \kappa \pi v_F^2 q^2 \bar{n}^2 |F_1^a|^2 \delta(\omega^2 - \omega_q^2), \qquad (7.16)$$

which will induce a spin resonance in all directions. It is worth it to note that in the spin channel, the isotropy in this dispersion relation at small $\vec{q}$ persists even deeper in the ordered phase.

B. 3D α phase for $l=1$

In the 3D α phase, we assume the Fermi-surface distortion along the z axis and the order-parameter configuration as $n^{\mu a} = \bar{n} \delta_{\mu,z} \delta_{a,3}$. Similar to the 2D case, the spin-up and -down Fermi surfaces are related by an overall shift at the wave vector $\vec{K} = 2\bar{n}/v_F \hat{z}$. The remaining symmetry is $SO_L(2) \otimes SO_S(2)$, which results in four Goldstone modes. They can be classified as two density channel modes and two spin channel modes. Without loss of generality, we choose the propagation wave vector $\vec{q}$ lying in the xz plane.

The density channel Goldstone modes describe the Fermi-surface oscillations in the x and y directions, which are associated with the fields $n_{z,1}$ and $n_{z,2}$. By a Legendre transformation, they are conjugate to the bilinear operators $Q_{z,1}$ and $Q_{z,2}$:

$$Q_{z1}(\vec{r}) = \psi_\alpha^\dagger(\vec{r})[\sigma_{z,\alpha\beta}(-i\nabla_x)]\psi_\beta(\vec{r}),$$

$$Q_{z2}(\vec{r}) = \psi_\alpha^\dagger(\vec{r})[\sigma_{z,\alpha\beta}(-i\nabla_y)]\psi_\beta(\vec{r}). \qquad (7.17)$$

Following the same procedure of the calculation in two dimensions, we find that the fluctuation kernel of the Goldstone mode $n_{z,1}$ is

$$L_{z1} = \kappa q^2 - i\frac{\pi}{4}N(0)s\cos^2\theta_q + N(0)s^2\cos 2\theta_q. \quad (7.18)$$

It is overdamped almost everywhere, except if $\vec{q}$ lies in the equator ($\theta = \pi/2$), in which case it is underdamped and has a quadratic dispersion. On the other hand, the fluctuation kernel of the Goldstone mode of $n_{z,2}$ reads

$$L_{z,2} = \kappa q^2 - iN(0)s\frac{\pi}{4}, \qquad (7.19)$$

which has no dependence on the angle θ_q. Hence, this mode is overdamped on the entire Fermi surface.

The spin channel Goldstone modes of $n_{x\pm iy,3}$ in the F_1^a channel behave similarly to that in the 2D case. We simply present their fluctuation kernels at small wave vectors as

$$L_{x\pm iy,3}(\vec{q},\omega) = \kappa q^2 - \frac{3N(0)}{|F_1^a|}s^2, \qquad (7.20)$$

where $s = \omega/v_F|K|$. The spin-wave excitation is also dressed by the interaction in the F_1^a channel in the α phase. By a similar calculation to the 2D case, we have

$$\chi_s(\vec{q},\omega) = \langle S_+(\vec{q},\omega)S_-(-\vec{q},-\omega) \rangle = \frac{|\chi_s^0(\vec{q},\omega)|^2}{L_{x+iy,3}(\vec{q},\omega)}. \qquad (7.21)$$

Thus, it also develops the same pole as in the spin channel Goldstone modes.

VIII. GOLDSTONE MODES IN THE β PHASES

In this section, we calculate the Goldstone modes and spin-wave spectra in the β phase at two and three dimensions at the RPA level. We will show that for $l=1$, a Lifshitz-like instability arises, leading to a spatially inhomogeneous ground state. This is because of a dynamically generated Dzyaloshinskii-Moriya interaction among the Goldstone modes as a result of the spontaneously breaking of parity. A GL analysis is presented to analyze this behavior.

A. 2D β phases

Without loss of generality, we consider the β phase in the F_l^a channel. We first assume a uniform ground state with the configuration of the d vector $\vec{d} = (\cos l\theta, \sin l\theta, 0)$ as defined in Eq. (4.6). The corresponding order parameter, i.e., the Higgs mode n_{Higgs}, is conjugate to operator O_{Higgs} as

$$O_{\text{Higgs}}(\vec{r}) = \frac{1}{\sqrt{2}}[Q_{x,1}(\vec{r}) + Q_{y,2}(\vec{r})]. \qquad (8.1)$$

By performing a relative spin-orbit rotation around the z, x, and y axes on the mean-field ansatz, we obtain the operators for three branches of Goldstone modes as

$$O_x(\vec{r}) = \frac{1}{\sqrt{2}}[Q_{x,2}(\vec{r}) - Q_{y,1}(\vec{r})],$$

$$O_x(\vec{r}) = -Q_{z,2}(\vec{r}), \quad O_y(\vec{r}) = Q_{z,1}(\vec{r}). \qquad (8.2)$$

We define the propagation wave vector of Goldstone modes $\vec{q}$ and its azimuthal angle ϕ, as depicted in Fig. 8. For the general direction of $\vec{q}$, it is more convenient to set up a frame with three axes x', y', and z, where $x' \parallel \vec{q}$ and $y' \perp \vec{q}$. We rotate O_x and O_y into

$$O_{x'} = \cos l\phi O_x - \sin l\phi O_y,$$

$$O_{y'} = \sin l\phi O_x + \cos l\phi O_y. \qquad (8.3)$$

O_z, $O_{x'}$, and $O_{y'}$ are the generators of a relative spin-orbit rotation around the z, x', and y' axes, respectively. Thus, in the following, we call the Goldstone mode of $O_{x'}$ the longitudinal Goldstone mode, and those of O_z and $O_{y'}$ are two transverse Goldstone modes.

The system with $\vec{d} = (\cos l\phi, \sin l\phi, 0)$ has the following reflection symmetry even in the presence of the $\vec{q}$;

$$\theta_k \to 2\phi - \theta_k, \quad \sigma_z \to -\sigma_z,$$

$$\sigma_x \to \sigma_x \cos 2l\phi + \sigma_y \sin 2l\phi,$$

$$\sigma_y \rightarrow \sigma_x \sin 2l\phi - \sigma_y \cos 2l\phi. \tag{8.4}$$

O_z and $O_{y'}$ are even under this transformation, while $O_{x'}$ is odd. Thus, $O_{x'}$ decouples from $O_{y'}$ and O_z, while hybridization occurs between O_z and $O_{y'}$. For a small wave vector, $\frac{v_F q}{\bar{n}} \ll 1$, and low frequency, $\frac{\omega}{\bar{n}} \ll 1$, we can ignore the mixing between the Goldstone modes and other gapped modes. For $l \geq 2$, the eigenvalues of the fluctuation kernel for the Goldstone modes are

$$L_{zz}(q,\omega) \approx L_{x'x'}(q,\omega) \approx L_{y'y'}(q,\omega) \approx \kappa q^2 - \frac{\omega^2}{4\bar{n}^2} \frac{N(0)}{|F_l^a|}, \tag{8.5}$$

where we have neglected the anisotropy among the three dispersion relations. A finite hybridization between O_z and $O_{y'}$ appears at the order of $O(q^l)$,

$$L_{zy'}(q,\omega) \propto iq^l, \tag{8.6}$$

which is negligible at small q at $l > 2$. Thus, the spectrum of the Goldstone modes is linear for $l > 2$. For $l = 2$, the hybridization is quadratic in $\vec{q}$,

$$L_{zy'}(q,\omega) = -i\frac{N(0)}{32\sqrt{2}k_F^2}q^2(1 + 4b) \ll \kappa q^2, \tag{8.7}$$

and thus must be taken into account. The resulting eigenmodes in the transverse channel are $O_z \pm iO_{y'}$. However, the linear dispersion relation remains at $l = 2$.

Similar to ferromagnets, there are two Fermi surfaces with unequal volume in the β phases. The interband transition has a gap of $2\bar{n}$ and a particle-hole continuum of width $2v_F q$, as depicted in Fig. 9. The Goldstone modes correspond to the interband transition with a velocity $v_{gs} \simeq 2\bar{n}\sqrt{\kappa|F_l^a(0)|/N(0)}$, and no Landau-damping effects exist at small q. Naturally, after Goldstone modes enter the particle-hole continuum, at the wave vector $q' \approx 2\bar{n}/(v_{gs} + v_F)$, the mode is no longer long lived and becomes Landau damped.

The linear dispersion relation of the Goldstone modes holds for all the values at $l \geq 2$. This feature is also due to the symmetry properties of the $n^{\mu a}$ under TR and parity transformation. The reasoning here is the same as that for the α phase in Sec. VII A.

We next calculate the spin-wave spectra in the β phase at $l \geq 2$. We have the following commutation relations:
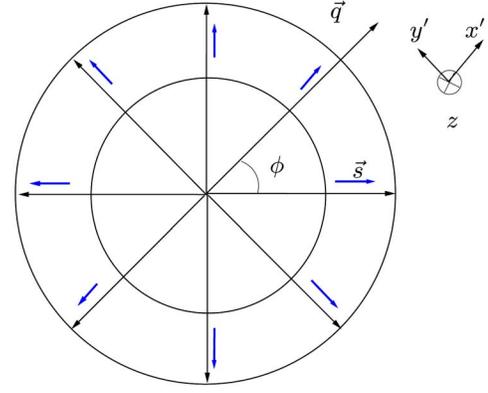
$$[S_+e^{i\phi_q}, e^{-i\phi_q}(O_x - iO_y)/\sqrt{2}] = iO_{Higgs} + O_z,$$

$$[S_x, O_z] = iO_{Higgs}. \tag{8.8}$$

The effective coupling between S_z and O_z can be calculated as

$$\chi^0_{Sz}(\vec{q},\omega) = \frac{-i}{\sqrt{2}} \frac{\omega}{\bar{n}} \frac{N(0)}{|F_l^a|} + O(q^2). \tag{8.9}$$

Thus, the spin-spin correlation function, dressed by the F_l^a channel interactions, near the resonance of the dispersing transverse collective mode has the form,

$$l = 1, w = 1$$

FIG. 8. (Color online) The three Goldstone modes of O_z, $O_{x'}$, $O_{y'}$ of the 2D β phase can be viewed as a relative spin-orbit rotation for this phase with angular momentum $l = 1$ and winding number $w = 1$. Here, ϕ is the azimuthal angle of the propagation direction $\vec{q}$.

$$\chi_s(\vec{q},\omega) = \langle S_z(\vec{q},\omega)S_z(-\vec{q},-\omega)\rangle = \frac{|\chi_s^0|^2}{L_{zz}(\vec{q},\omega)}$$

$$= \frac{2N(0)}{|F_l^a|} \frac{\omega^2}{\omega^2 - 4\bar{n}^2 \frac{|F_l^a|}{N(0)}\kappa q^2}. \tag{8.10}$$

The spectral function at the resonance reads

$$\text{Im }\chi_s(\vec{q},\omega) = 8\bar{n}^2\kappa q^2 \delta(\omega^2 - \omega_q^2). \tag{8.11}$$

Similarly, the effective coupling between $S_+e^{i\phi_q}$ and $e^{-i\phi_q}(O_x - iO_y)/\sqrt{2}$ gives the same result,

$$\chi^0_{s_{x\pm iy}} = \chi^0_{sz}. \tag{8.12}$$

The transverse spin-spin correlation function is

$$\langle S_+(\vec{q},\omega)S_-(-\vec{q},-\omega)\rangle = \frac{|\chi^0_{s_{x\pm iy}}|^2}{L_{x+iy,x-iy}}, \tag{8.13}$$

which is also dressed by the interactions.

B. Lifshitz-like instability in the 2D p-wave channel

For $l = 1$, with the assumption of the uniform ground state, the dispersion for the longitudinal mode O_z remains linear as

$$\omega_L^2 = 4\bar{n}^2|F_1^a|\frac{\kappa}{N(0)}q^2. \tag{8.14}$$

However, the situation for the transverse modes is dramatically different. The mixing between O_z and $O_{y'}$ scales linearly with q:

$$L_{zy'}(\vec{q},\omega) = -L_{y'z}(\vec{q},\omega) \approx \frac{i}{4\sqrt{2}}\left(b + \frac{3}{2}\right)N(0)x\frac{q}{k_F}.$$

$$(8.15)$$

We diagonalize the matrix and then obtain the eigenmodes as $O_z \pm iO_{y'}$ with the following dispersion relation:

$$\omega_{T,\pm}^2 = 4\bar{n}^2|F_1^a(0)|\left[\frac{\kappa q^2}{N(0)} \pm cx\frac{q}{k_F}\right], \qquad (8.16)$$

as depicted in Fig. 10 where c is a constant at the order of 1.

Clearly, $\omega_{T,-}^2 < 0$ for small $|\vec{q}|$. This means that the uniform ground state cannot be stable in the F_1^a channel due to a Lifshitz-like instability.[59,60] This instability can be understood in terms of the nontrivial effects of the gradient term with coefficient γ_2 in the GL free energy in Eq. (3.5). This term is cubic in the order parameter $n^{\mu,b}$ and linear in spatial derivatives. This term leads to an inhomogeneous ground state in the β phase, in which parity is spontaneously broken. A similar phenomenon occurs in the bent-core liquid-crystal system, where a spontaneously chiral inhomogeneous nematic state arises in a nonchiral system. A similar term involving a linear derivative and the cubic order of order parameter is constructed in Ref. 61 to account for this transition. These inhomogeneous ground states also occur in chiral liquid crystal[6] and helimagnets[43] such as MnSi, in which parity is explicitly broken. In contrast, such a term is prohibited in the ferromagnetic transition[44,45] and the nematic-isotropic phase transition[4] in the density channel Pomeranchuk instabilities. We will see that the GL analysis below based on the symmetry argument agrees with the RPA calculations in Eq. (8.6).

In order to obtain the values of $\gamma_{1,2}$, we linearize the gradient terms in Eq. (3.5) in the ground state with d-vector configuration of $\vec{d} = (\cos\theta, \sin\theta, 0)$, i.e.,

$$\vec{n}_1 = \sqrt{\bar{n}^2 - \delta n_1^2}\,\hat{e}_x + \delta\vec{n}_1,$$

$$\vec{n}_2 = \sqrt{\bar{n}^2 - \delta n_2^2}\,\hat{e}_y + \delta\vec{n}_2, \qquad (8.17)$$

where $\delta\vec{n}_1 \perp \hat{e}_x$, $\delta\vec{n}_2 \perp \hat{e}_y$, and $\vec{n}_1 \perp \vec{n}_2$ are kept. The contribution from the Goldstone modes can be organized into

$$F_{grad}(\vec{O}) = \gamma_1[(\partial_i O_x)^2 + (\partial_i O_y)^2 + (\partial_i O_z)^2] + \frac{\gamma_2\bar{n}}{\sqrt{2}}(O_x\partial_y O_z$$

$$- O_y\partial_x O_z) + \gamma_2\bar{n}^2(\partial_x O_x + \partial_y O_y). \qquad (8.18)$$

With the assumption of the uniform ground state, the first γ_2 term behaves like a Dzyaloshinskii-Moriya term, and gives a linear dependence in the dispersion relation as appears in Eq. (8.16). By matching the coefficients, we arrive at the result,

$$\gamma_1 = \kappa, \qquad \gamma_2 = \frac{\sqrt{2}cN(0)}{v_F k_F^2}. \qquad (8.19)$$

The second coefficient γ_2 in the GL expansion of Eq. (8.18) is a total derivative of the longitudinal Goldstone modes. It does not contribute to the equation of motion for the Goldstone modes around the saddle point of the uniform mean-field ansatz. However, Eq. (3.5) actually allows a
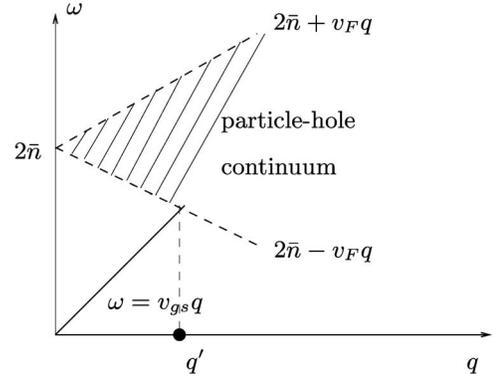

FIG. 9. The linear dispersion relation of Goldstone modes of the 2D β phases ($l \geq 2$) at small momentum $\vec{q}$. For $q > q'$, the Goldstone modes enter the particle-hole continuum, and are damped.

twisted ground state in the longitudinal channel, as depicted in Fig. 11(a). Without loss of generality, we assume a pitch vector along the x axis, $\vec{q} \| \hat{x}$, and perform a longitudinal twist of the Goldstone configuration of $\vec{n}_{1,2}$ as

$$\vec{n}_1 = \bar{n}(1,0,0), \quad \vec{n}_2 = \bar{n}(0,\cos qx, -\sin qx). \quad (8.20)$$

This configuration means that we fix $\vec{n}_1$ and rotate $\vec{n}_2$ around the x axis. If the system has a small external spin-orbit coupling, it pins the order-parameter configuration. We introduce an effective spin-orbit field h_{so} to describe this effect:

$$V(h_{so}) = -h_{so}(n_{x,1} + n_{y,2}). \qquad (8.21)$$

Then, the GL free energy becomes

$$F(n) = \gamma_1\bar{n}^2 q^2 - \gamma_2\bar{n}^3 q - h_{so}\bar{n}\cos qx. \qquad (8.22)$$

If h_{so} is less than a critical value $h_{so,L}$ defined as

$$h_{so,L} = \frac{\gamma_2^2\bar{n}^3}{4\gamma_1}, \qquad (8.23)$$

then the Lifshitz instability occurs with the pitch of $q_c = \gamma_2\bar{n}/(2\gamma_1)$. If $h_{so} > h_{so,L}$, the instability due to the longitudinal Goldstone mode is suppressed.

Now let us look at the instability caused by the transverse Goldstone modes, as depicted in Fig. 11(b). The transverse mode $O_z + iO_y$ describes the precession of the triad of $\hat{n}_1$, $\hat{n}_2$, $\hat{n}_3 = \hat{n}_1 \times \hat{n}_2$ as

$$\vec{n}_1 = \bar{n}(\cos\epsilon\,\hat{e}_x + \sin\epsilon\cos qx\,\hat{e}_y - \sin\epsilon\sin qx\,\hat{e}_z),$$

$$\vec{n}_2 = \bar{n}\left[-\sin\epsilon\cos qx\,\hat{e}_x + \left(\cos^2\frac{\epsilon}{2} - \sin^2\frac{\epsilon}{2}\cos 2qx\right)\hat{e}_y\right.$$

$$\left. - \sin^2\frac{\epsilon}{2}\sin 2qx\,\hat{e}_z\right], \qquad (8.24)$$

where ϵ describes the precession amplitude, $\vec{n}_1$ precesses around the x axis, and $\vec{n}_2$ traces a "figure of eight" orbit on the surface of the unit sphere. To linear order of ϵ, the free-energy cost is
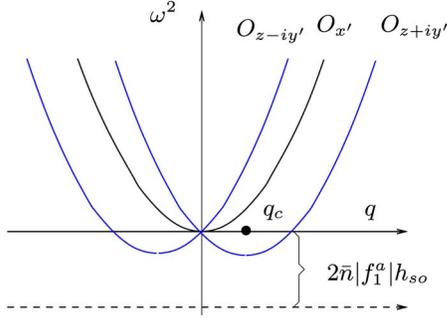
FIG. 10. (Color online) The dispersion relation of Goldstone modes for the β phase with $l=1$. The longitudinal modes $O_{y'}$ have linear dispersion relation, while the two transverse modes $O_{z\pm iy'}$ are unstable toward the Lifshitz-like instability at small momentum $\vec{q}$.

$$V(n) = \frac{3}{2}\gamma_1 q^2 (\bar{n}\epsilon)^2 + \frac{\bar{n}}{2}q\gamma_2(\bar{n}\epsilon)^2 + \frac{h_{so}}{\bar{n}}\frac{3}{4}(\bar{n}\epsilon)^2. \quad (8.25)$$

Hence, when h_{so} is larger than a critical value $h_{so,T} = \gamma_2^2\bar{n}^3/18\gamma_1 < h_{so,L}$, the instability due to the transverse Goldstone modes is suppressed.

Because $h_{so,L} > h_{so,T}$, the longitudinal Goldstone channel instability is stronger than that in the transverse channel. Thus, in the absence of the external field, the ground state exhibits the longitudinal twist of Eq. (8.20). However, this spiral order cannot give static Bragg peaks in neutron-scattering experiments as occurs in the case of a helimagnet, although it can couple to the spin-spin correlations through a dynamic effect. However, the spatial inhomogeneity complicates the calculation. This remains an interesting problem, which we will not pursue further in this work.

If $h_{so} \gtrsim h_{so,L}$, then both instabilities are suppressed, and thus, in this regime, the ground state is uniform. In this case, the Goldstone spectrum has an overall shift based on Eq. (8.18) as

$$\omega'^2_l = \omega_l^2 + 2|f_1^a|\bar{n}h_{so}, \quad \omega'^2_t = \omega_t^2 + 2|f_1^a|\bar{n}h_{so}, \quad (8.26)$$

as depicted in Fig. 10. Then, the spectra for the two transverse Goldstone modes exhibit a rotonlike structure with a gap of

$$\Delta = \sqrt{2\bar{n}|f_1^a|(h_{so} - h_{so,T})}, \quad (8.27)$$

at $q'_c = \gamma_2\bar{n}/(4\sqrt{2}\gamma_1)$.

C. Goldstone modes in the 3D β phase

For the 3D β phase, we only consider the case of $l=1$ with the ground-state configuration of the d vector as $\vec{d}(\vec{k}) \| \vec{k}$. The Goldstone modes behave similarly to the 2D case. The Legendre conjugation operators of the order parameter $n^{\mu,b}$ can be decomposed into the operators O_{J,J_z} ($J=0,1,2;J_z=-J,\ldots J$) as eigenoperators of the total angular momentum $\vec{J}=\vec{L}+\vec{S}$ in the β phase. The Higgs mode carries $J=0$ defined as
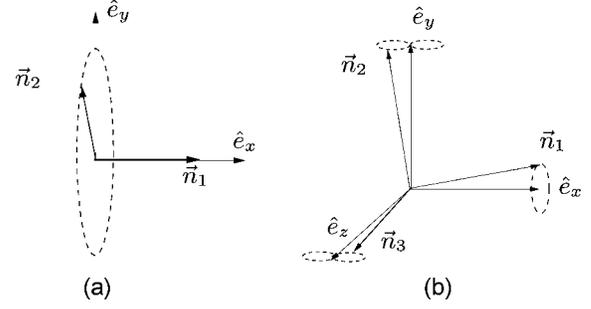

FIG. 11. Longitudinal and transverse twists for the Lifshitz-like instability in the β phase with $l=1$. (a) The longitudinal twist with $\hat{n}_2$ precessing around the $\hat{e}_1$ axis, as described in Eq. (8.20). (b) The transverse twist with the triad formed by $\hat{n}_1$, $\hat{n}_2$, and $\hat{n}_3 = \hat{n}_1 \times \hat{n}_2$ precessing around the $\hat{e}_x$ axis, as described in Eq. (8.24).

$$O_{\text{Higgs}}(\vec{r}) = \frac{1}{\sqrt{3}}\delta_{\mu a}n^{\mu a}(\vec{r}). \quad (8.28)$$

Due to the broken relative spin-orbit symmetry, the relative spin-orbit rotations generate the three Goldstone modes O_x, O_y, and O_z,

$$\hat{O}_i(\vec{r}) = \frac{1}{\sqrt{2}}\epsilon_{i\mu a}n^{\mu,a}(\vec{r}), \quad (8.29)$$

which carry total angular momentum $J=1$. We choose the propagation wave vector $\vec{q}$ along the z axis. Due to presence of $\vec{q}$, only J_z is conserved. The relation between O_x, O_y, and O_z and those in the helical basis $O_{1,\pm1}$ and O_{10} is

$$O_{1,\pm1} = \frac{1}{\sqrt{2}}(O_x \pm iO_y), \quad O_{1,0} = O_z. \quad (8.30)$$

In the low frequency and small wave vector regime as $\omega, v_F q \ll \bar{n} \ll v_F k_F$, we can neglect the mixing between Goldstone modes and other massive modes. Similar to the case in two dimensions, we calculate the fluctuation kernels of the Goldstone modes as

$$L_{10,10}(q,\omega) = \kappa q^2 - \frac{\omega^2}{4\bar{n}^2|f_1^a|}, \quad (8.31)$$

$$L_{1\pm1,1\pm1}(q,\omega) = \kappa q^2 \pm \frac{N(0)}{18}\frac{q}{k_F}x - \frac{\omega^2}{4\bar{n}^2|f_1^a|}. \quad (8.32)$$

For simplicity, we have neglected the anisotropy in the q^2 term in Eq. (8.32). Their spectra read

$$\omega_{j_z}^2 = 4\bar{n}^2|F_1^a|\left[\frac{\kappa q^2}{N(0)} + j_z\frac{|q|x}{18k_F}\right] \quad (j_z = 0, \pm 1). \quad (8.33)$$

Because of the broken parity, the channel of $j_z=-1$ is unstable, which leads to the Lifshiz-like instability as discussed in the 2D β phase.

Again this Lifshitz instability is due to the nontrivial γ_2 term in the GL free energy of Eq. (3.12). To determine the coefficients of the gradient terms, we linearize the γ_2 term around the saddle point, and define the deviation from the uniform mean-field ansatz as

$$\vec{n}_1 = \sqrt{\bar{n}^2 - \delta n_1^2}\hat{e}_x + \delta\vec{n}_1, \quad \vec{n}_2 = \sqrt{\bar{n}^2 - \delta n_2^2}\hat{e}_y + \delta\vec{n}_2,$$

$$\vec{n}_3 = \sqrt{\bar{n}^2 - \delta n_3^2}\hat{e}_z + \delta\vec{n}_3, \quad (8.34)$$

where $\delta\vec{n}_1 \perp \hat{e}_x$, $\delta\vec{n}_2 \perp \hat{e}_y$, and $\delta\vec{n}_3 \perp \hat{e}_z$. The contribution from the Goldstone modes becomes

$$F_{grad}(O) = \gamma'_1[(\partial_i O_x)^2 + (\partial_i O_y)^2 + (\partial_i O_z)^2] - \frac{\gamma'_2}{2}\bar{n}\epsilon_{ijk}O_i\partial_j O_k$$

$$+ \gamma'_2\sqrt{2}\bar{n}^2\partial_i O_i. \quad (8.35)$$

Similar to the 2D case, the values of γ'_1 and γ'_2 can be determined by matching the coefficients of the dispersion relation in Eq. (2.5) as

$$\gamma'_1 \approx \kappa, \quad \gamma'_2 = \frac{N(0)}{18v_F k_F^2}, \quad (8.36)$$

where the difference among the three Franck constants is neglected.

Following the same procedure in the 2D case in Sec. VIII B, we study the instabilities of the longitudinal and transverse twists in the 3D β phase with an external spin-orbit field to pin the order parameter,

$$V_{so} = -h_{so}^{3D}(n^{x,1} + n^{y,2} + n^{z,3}). \quad (8.37)$$

After a straightforward calculation, we find that longitudinal twist occurs at the pitch wave vector $q_{L,3D} = \bar{n}\gamma_2/(2\gamma_1)$ with a critical value of h_{so}^{3D} field to suppress the twist at $h_{so,L}^{3D} = \gamma_2^2\bar{n}^3/(4\gamma_1)$, and those of the transverse twist are $q_{T,3D} = q_{L,3D}/2$ and $h_{so,T}^{3D} = h_{so,L}/2$. Thus, the conclusion that the instability of the longitudinal twist is stronger than that of the transverse twist is the same as in the 2D case. Again, if $h_{so}^{3D} \geq h_{so,L}^{3D}$, then the ground state is uniform, and the spectrum of the two transverse Goldstone modes exhibits a rotonlike structure with a gap

$$\Delta = \sqrt{2\bar{n}|f_1^a|(h_{so} - h_{so,T})}, \quad (8.38)$$

located at $q_{T,3D}$.

IX. MAGNETIC-FIELD EFFECTS AT ZERO TEMPERATURE

In this section, we discuss the magnetic-field effect to the order-parameter configurations in the α and β phases. Due to the symmetry constraint, the $\vec{B}$ field does not couple to the order parameter $n^{\mu a}$ linearly, and the leading-order coupling begins at the quadratic level as

$$\Delta F(\vec{B}, \vec{n}_b) = (u + w)g^2 B^2 \text{tr}[n^T n] - wg^2 B^\mu B^\nu n^{\mu b} n^{\nu b}$$

$$= ug^2 B^2 \sum_b n_b^2 + wg^2 \sum_b (\vec{B} \times \vec{n}_b)^2, \quad (9.1)$$

with g the gyromagnetic ratio. The coefficients u and w can be determined from the microscopic calculation by using the mean-field approach as

$$u = 4v_1 - 2v_2, \quad w = 4v_2 \quad \text{(at two dimensions)},$$

$$u = 6v_1 - 3v_2, \quad w = 5v_2 \quad \text{(at three dimensions)}, \quad (9.2)$$

with $v_{1,2}$ defined in Eq. (4.12) in two dimensions and Eq. (4.19) in three dimensions, respectively. v_1 is usually larger than v_2; thus, u is typically positive. This means that the external $\vec{B}$ field suppresses the magnitude of order parameters as

$$\bar{n}(B) = \bar{n}(B = 0)\sqrt{1 - \frac{B^2}{B_c^2}} \quad (9.3)$$

in both α and β phases, where the critical value of B_c is defined as

$$\frac{\mu_B B_c}{v_F k_F} = \frac{\sqrt{\frac{|r|}{u}}}{v_F k_F} = \frac{\bar{n}(0)}{k_F v_F} \ll 1. \quad (9.4)$$

This effect has been studied in Ref. 32.

In the α phase, w is positive. Thus, the spin components of the order parameter of this phase, $\vec{n}_b$, prefer to be parallel or antiparallel to the magnetic field $\vec{B}$. Consequently, the Fermi surface with its spins polarized parallel to the magnetic field becomes larger in size than the Fermi surface for the spins pointing in the opposite direction. In the case of the nematic-spin-nematic phase, the α phase with angular momentum $l=2$, the main effect of the magnetic field is to break the symmetry by $\pi/2$ rotations, i.e., a spatial rotation followed by a spin reversal, while retaining the symmetry under rotations by π (Fig. 12). Thus, the magnetic field induces a nonzero component of the charge nematic order parameter, the nematic in the spin-singlet channel. (Analogs of this effect hold in all angular momentum channels.) On the other hand, for a translation and rotationally invariant system, the Fermi-surface distortion, i.e., orientation of the order parameter in real space, cannot be locked to the direction of the $\vec{B}$ field. As a result, the Goldstone manifold becomes $[SO_S(2) \otimes SO_L(2)]/SO_S(2) = SO_L(2)$.

The B field in the β phase also constrains the direction of the vectors $\vec{n}_b$. Since w is negative in the β phase, $\vec{B}$ prefers to be perpendicular to $\vec{n}_b$ vectors. Thus, in the 2D system, $\vec{n}_1$, $\vec{n}_2$, and $\vec{B}$ form a triad, which can be either left handed or right handed, as depicted in Fig. 13. The spin configuration on Fermi surfaces changes from a large circle into two smaller circles with a net spin polarization along the $\vec{B}$ field. The triad still has the degrees of freedom to rotate around the axis of $\vec{B}$; thus the Goldstone manifold at two dimensions is reduced from $SO_{L+S}(3)$ to $SO_{L+S}(2) \times Z_2$. The B field effect in 3D systems is more subtle. At small values of B, $\vec{n}_1$, $\vec{n}_2$, and $\vec{n}_3$ can no longer form a triad with $\vec{B}$. Instead, $\vec{n}_1$, $\vec{n}_2$, and $\vec{n}_3$ form a distorted triad with the direction of the distortion lying in the diagonal direction and parallel to $\vec{B}$, as depicted in Fig. 14(a). As B grows larger, the three vectors $\vec{n}_1$, $\vec{n}_2$, and $\vec{n}_3$ are pushed toward the plane perpendicular to $\vec{B}$. For B larger than a value B', defined as

$$B' = B_c \sqrt{\frac{v_2}{v_2 + 4|w|v_1/u}}, \qquad (9.5)$$

$\vec{n}_1$, $\vec{n}_2$, and $\vec{n}_3$ become coplanar, and with a relative angle of $2\pi/3$, i.e., an equilateral triangle, as depicted in Fig. 14(b). If B is further increased, $\vec{n}_1$, $\vec{n}_2$, and $\vec{n}_3$ keep these directions but their magnitudes continuously shrink to zero at $B=B_c$.

We next discuss the effect of magnetic field B on the Lifshitz-like instability in the 2D β phase at $l=1$. We assume that $\vec{B}$ is parallel to the z direction. As shown in Sec. VIII B, the instability of the longitudinal twist described in Eq. (8.20) is stronger than that of the transverse twist. Thus, we will focus here on the case of the longitudinal twist. In this case, the order parameter $\vec{n}_2$ precesses around the $\hat{e}_1$ axis. Thus, $\vec{B}$, $\vec{n}_1$, and $\vec{n}_2$ cannot form a fixed triad uniformly in space. The free energy of Eq. (3.5) now becomes

$$V(n) = \gamma_1 \bar{n}^2 q^2 - \gamma_2 \bar{n}^3 q - wB^2 \bar{n}^2 (1 + \cos^2 qx). \quad (9.6)$$

Hence, for B larger than a critical value of B_{cl},

$$B_l = \frac{B_c}{\sqrt{1 + 8v_1|w|\gamma_1/(u\gamma_2^2)}}, \qquad (9.7)$$

the Lifshitz instability of the β phase to a phase with a longitudinal twist is suppressed. The effects of an external B field in the 3D β phase are more complicated and will not be discussed here.

Finally, we note that the order parameter $n^{\mu a}$ can couple to the magnetic field B linearly when other external fields are also present. For $l=1$, a possible additional term in the free energy is of the form,

$$\Delta F(B,j) = \gamma_3 B^\mu j_a(\vec{r}) n^{\mu,a}, \qquad (9.8)$$

where j_a is the ath component of the electric current. To the leading order, the mean-field value of the coupling constant γ_3 is

$$\gamma_3 = -\frac{\hbar^2 e \mu_B}{2m^* v_F} \frac{N(0)}{v_F k_F}, \qquad (9.9)$$

where m^* is the effective mass and e is the charge of electrons. For $l=2$, a similar term can be constructed as

$$\Delta F(B,u) = \gamma_4 B^\mu u_a(\vec{r}) n^{\mu,a}, \qquad (9.10)$$

where u_a is the strain field. Due to these terms, in the α phase, the electric current and lattice strain can be used to lock the direction of the order parameter in real space in the presence of an external magnetic field at $l=1$ and $l=2$, respectively. In the β phase, this term will distort the round Fermi surfaces into two orthogonal ellipses but with different volumes.

X. SPIN CURRENT INDUCED BY A CHARGE CURRENT IN THE *d*-WAVE CHANNEL

In the *d*-wave ($l=2$) case, the order parameters have the structure of the spin-quadruple moments. From the symmetry analysis, a spin current $J_s^{\mu,a}$ may be induced by a charge current J_c^a flowing through the system, where μ is the spin
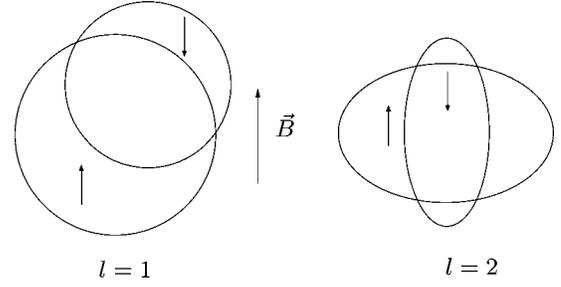

FIG. 12. The α phases in a $\vec{B}$ field ($l=1,2$). The larger Fermi surface has spin parallel to the $\vec{B}$ field. The Fermi-surface distortion is not pinned by the $\vec{B}$ field.

index and a,b are the spatial indices. For simplicity, we only study the 2D α and β phases. In the standard quadruple notation, the order parameters $n^{\mu,1}$ and $n^{\mu,2}$ can be represented as $n^{\mu,1}=n^{\mu,xx}-n^{\mu,yy}$ and $n^{\mu,2}=2n^{\mu,xy}=2n^{\mu,yx}$. Then, we write the formula as

$$J_s^{\mu,a} = g \bar{n}^{\mu,ab} J_c^b, \qquad (10.1)$$

where the matrix $\bar{n}^{\mu,ab}$ is related to the order parameter $\bar{n}^{\mu,a}$ as

$$\bar{n}^{\mu,ab} = 2 \begin{pmatrix} \bar{n}^{\mu,xx} & \bar{n}^{\mu,xy} \\ \bar{n}^{\mu,yx} & \bar{n}^{\mu,yy} \end{pmatrix} = \begin{pmatrix} \bar{n}^{\mu,1} & \bar{n}^{\mu,2} \\ \bar{n}^{\mu,2} & -\bar{n}^{\mu,1} \end{pmatrix}. \quad (10.2)$$

By the standard the linear-response theory, the coefficient g can be calculated as

$$g = \frac{(3-2a)\pi}{ek_F v_F |F_2^a|}. \qquad (10.3)$$

In the α phase, it is convenient to choose the direction of the axes of the reference frame x and y along the major and minor axes of the distorted Fermi surfaces, and assume spin quantization along the z axis, so that $\bar{n}^{\mu,ab}=\bar{n}\hat{e}_z \text{diag}\{1,-1\}$. A charge current J_c^a running along the major and minor axes induces a spin current $J_s^{\mu,a}$ flowing in the same (or opposite) direction. But for the general direction of J_c^a, the induced spin current $J_s^{\mu,a}$ flows with an angle with J_c^a. We denote the azimuthal angle between the charge current J_c^a and the x axis as ϕ. Then, the angle between J_c^a and $J_c^{\mu,a}$ reads 2ϕ or $\pi-2\phi$ depending on the sign of g. The nature of the induced spin current here is different from that of the spin Hall effect in semiconductors with SO coupling. In that case, the spin Hall current always flows perpendicular to the electric field, and the spin Hall conductance is invariant under time-reversal transformation. Here, because of the anisotropy of the Fermi surfaces, the spin current is perpendicular to the charge current, only if the charge current flows along the diagonal direction ($\phi=\pm\pi/4, \pm3\pi/4$). On the other hand, the *d*-wave phases break time-reversal symmetry; thus, the induced spin current is not dissipationless.

In the β phase, without loss of generality, we can take the order-parameter configuration as in Fig. 3(a), i.e.,
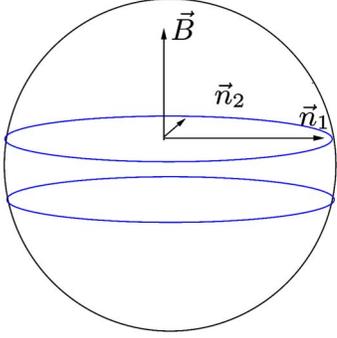
FIG. 13. (Color online) The spin configuration on the Fermi surfaces in the β phase (F_l^a channel). With the $\vec{B}$ field, the large circle splits into two small circles perpendicular to the $\vec{B}$ field with the development of a finite magnetization. The large (small) Fermi surface polarizes parallel (antiparallel) to the $\vec{B}$ field.

$$n^{\mu,ab} = \bar{n}\begin{pmatrix} \hat{e}_x & \hat{e}_y \\ \hat{e}_y & -\vec{e}_x \end{pmatrix}, \qquad (10.4)$$

where $\hat{e}_{x,y}$ denote the spin direction. We assume that the charge current J_c^a flows along the x direction. Then, two spin currents polarizing along orthogonal directions are induced with the same magnitude. The spin current flowing along the x direction polarizes along $\hat{e}_x$, while that flowing along the y direction polarizes along $\hat{e}_y$. If we measure the spin current along the spatial direction with the azimuthal angle ϕ with respect to the x axis, the induced spin current along this direction polarizes along the direction of $\cos\phi\hat{e}_x + \sin\phi\hat{e}_y$. Because in the β phase, there is an induced SO coupling, spin and orbital angular momenta will not be preserved separately. As a result, it is impossible in the β phase to describe a spin current by two separated indices (a spatial index and a spin one). The spatial degrees of freedom and the spin ones must be mixed together.

Finally, in a real material, there would always be some SO coupling. With even an infinitesimal SO coupling, a charge current flowing inside the system can remove the degeneracy of the ground states in the ordered phase. In other words, in the presence of explicit SO interactions, a charge current can pin down the direction of the order parameter. Therefore, the
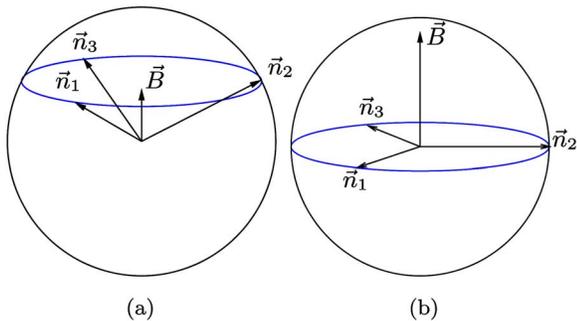
relative angle between the order parameter and the charge current is not arbitrary. As a result, to be able to adjust the angle between the charge current and the order parameter as we mentioned above, some other mechanism is necessary to pin down the order parameter such that the order parameter will not rotate when we rotate the direction of the charge current. For example, an in-plane magnetic field or a lattice potential as background can do the job.

XI. POSSIBLE EXPERIMENTAL EVIDENCE FOR THESE PHASES

At the present time, we are not aware of any conclusive experimental evidence for a spin-triplet channel Pomeranchuk instability. However, the α and β phases presented here are just a natural generalization of ferromagnetism to higher partial-wave channels. Taking into account the existence of the p-wave Cooper pairing phase in the ^{3}He systems[1] and the strong evidence for its existence in the ruthenate compound Sr_2RuO_4,[62] we believe that there is a strong possibility of finding these phases in the near future. Basically, the driving force behind the Pomeranchuk instabilities in the spin-triplet channels is still the exchange interaction among electrons, which shares the same origin as in ferromagnetism. Although the weak coupling analysis we have used here may not apply to the materials of interest, as many of them are strongly correlated systems, many of the symmetry issues will be the same as the ones we have discussed here, with the exception of the role of lattice effects, which we have not addressed in detail and which may play a significant role, i.e., by gapping out many of the Goldstone modes associated with the continuous rotational symmetry of the models that we have discussed. Nevertheless the GL free energies will have much of the same form even if the actual coefficients may be different, since we typically need a strong enough exchange interaction in a non-s-wave channel. In the following, we will summarize a number of known experimental systems (and numerical), which suggest possible directions to search for the α and β phases.

(a) *^{3}He*. The spin-exchange interaction in the Fermi liquid state of ^{3}He is very strong, as exhibited in the low-frequency paramagnon modes.[1] In this system, the spin fluctuations are known to mediate the p-wave Cooper pairing. The Landau parameter F_1^a in ^{3}He was determined to be negative from various experiments,[63–66] including the normal-state spin diffusion constant, spin-wave spectrum, and the temperature dependence of the specific heat. It varies from around -0.5 to -1.2 with increasing pressures to the melting point. Although F_1^a is not negatively large enough to pass the critical point, we expect that reasonably strong fluctuation effects exist.

(b) *URu_2Si_2*. The heavy fermion compound URu_2Si_2 undergoes a phase transition at 17 K. The tiny antiferromagnetic moment developed in the low-temperature phase cannot explain the large entropy loss. About 40% density of state density is lost at low temperatures. Currently, the low-temperature phase is believed to be characterized by an unknown "hidden" order parameter.[67] An important experimen-

FIG. 14. (Color online) The order parameters in the 3D β phase at $l=1$. (a) Configuration for $B'>B$ as defined in Eq. (9.5). (b) Configuration for $B_c>B>B'$.

tal result of nuclear magnetic resonance[68] (NMR) shows the broadening of the line shape below T_c. This implies the appearance of a random magnetic field in the hidden ordered phase. Recently, Varma and Varma and Zhu proposed the p-wave α phase as the hidden ordered phase.[31,32] They fitted the specific-heat jump reasonably well, and more importantly the jump of the nonlinear spin susceptibility χ_3 at the transition. The origin of the random field in the NMR experiment is explained by the spin moment induced by disorder in the p-wave α phase. However, the α phase still has Fermi surfaces; thus, it is difficult to explain the large loss of density of states. Further, the α phase is time reversal even; thus, its coupling to spin moment must involve the B field. In the NMR experiment, an external B field is indeed added. It would be interesting to check whether the line-shape broadening is correlated with the magnitude of B.

(c) *$Sr_3Ru_2O_7$*. The bilayer ruthenate compound $Sr_3Ru_2O_7$ develops a metamagnetic transition in an applied magnetic field B perpendicular to the c axis. In very pure samples, for B from 7.8 to 8.1 T, the resistivity measurements show a strong enhancement below 1.1 K.[14] Transport measurements in tilted magnetic fields, with a finite component of the B field in the ab plane, show evidence for a strong in-plane temperature-dependent anisotropy of the resistivity tensor, which is suppressed at larger in-plane fields.[14,15] This effect is interpreted as a nematic transition for the Fermi surface of the majority spin component.[14] This result suggests a state, which is a superposition of both a charge nematic and a nematic-spin-nematic state. On the square lattice, the $d_{x^2-y^2}$ distortion pattern is more favorable than that of d_{xy}. Thus, the transition should be Ising-like. In the presence of SO coupling, while preserving both parity and TR symmetries, the magnetic field can couple to the $d_{x^2-y^2}$ channel order parameter through terms in the free energy of the form,

$$(B_x^2 - B_y^2)B_z n_{z,1},\qquad(11.1)$$

which is cubic in B, and

$$\vec{B}\cdot\vec{n}_a n_a \qquad(11.2)$$

(where n_a is the charge nematic order parameter), which is linear in B. Thus, an in-plane B field can lock the orientation of the nematic-spin-nematic order parameter. This effect is more pronounce if the system is in a charge nematic phase.

(d) *2DEG in large magnetic fields*. Currently, the strongest experimental evidence for a charge nematic (fully polarized) state is in the case of a 2DEG in a large perpendicular magnetic field.[11–13] In the second and higher Landau levels, a huge and strongly temperature-dependent resistance anisotropy is seen in ultrahigh mobility samples, for filling factors near the middle of the partially filled Landau level. In this regime, the I-V curves are clearly linear at low bias. No evidence is seen of a threshold voltage or of broadband noise, both of which should be present if the 2DEG would be in a stripe state, which is favored by Hartree-Fock calculations. Both effects are seen in nearby reentrant integer Hall states. Thus, the simplest interpretation of the experiments is that the ground state is a polarized charge nematic.[9,10] There is still a poorly understood alternation effect: the strength of

the anisotropic resistance appears to alternate between the fully polarized state and the state with partial polarization. Although this effect could be explained in terms of microscopic calculations of the order parameter, it is still possible that the latter may suggest some form of partially polarized nematic-spin-nematic order. There are no reliable calculations of Landau parameters in these compressible phases.

(e) *The 2DEG at zero magnetic field*. The 2DEG at low densities is a strongly coupled system and much work has been done on this system in the context of its apparent metal-insulator transition. What interests us is the possibility that this system may have phases of the type discussed here. (The possibility of nonuniform "microemulsion" phases in the 2DEG was proposed recently by Jamei *et al.*[69]) A numerical evaluation to the Landau parameter F_1^a in two dimensions, performed by Kwon *et al.*,[70] by using variational quantum Monte Carlo, found that F_1^a is negative and decreasing from -0.19 at $r_s=1$ to -0.27 at $r_s=5$. On the other hand, Raikh and co-workers[71,72] investigated the many-body renormalization effect to the Rashba SO coupling due to the exchange interaction in the F_1^a channel. They found the renormalized SO coupling is amplified significantly at large r_s by using a local-field approximation. More numerical work to check whether Pomeranchuk instabilities can occur in this system would be desirable.

(f) *Ultracold atomic gases with a p-wave Feshbach resonance*. Another type of strongly interacting system includes cold atoms with Feshbach resonances. Recently, an interspecies p-wave Feshbach resonance has been experimentally studied by using the two component ^6Li atoms.[73] In the regime of positive scattering length, close to the resonance, the Landau parameter of F_1^a should be negative and large in magnitude. Thus, this system would appear to be a good candidate to observe these phases. However, since the p-wave Feshbach resonance is subject to a large loss rate of particles, it is not clear whether it would be possible to use this approach to observe a stable system with a Pomeranchuk instability near the resonance.

(g) *How to detect these phases*. We also propose several experimental methods to detect the α and β phases (see also the discussion in Ref. 35). For the case of the spatially anisotropic α phases, evidence for strongly temperature dependent anisotropy in the transport-properties (as well as the tunability of this effect by either external in-plane magnetic fields and/or uniaxial stress) as seen in $Sr_3Ru_2O_7$ and in the 2DEG can provide direct evidence for the spatial nematic nature of these phases. Spatially nematic phases exhibit anisotropic transport properties even in a single-domain sample.[4] Their spin structure is more difficult to determine. Because no magnetic moments appear in both phases, elastic neutron scattering does not exhibit the regular Bragg peaks. Since the Goldstone modes are combined spin and orbital excitations, they cannot be directly measured through neutron scattering. Nevertheless, in the ordered phase, as we have discussed, spin-spin correlation function couples to the Goldstone modes and develops a characteristic resonance structure, which should be accessible to inelastic neutron scattering. An experimental detection of this resonance and its appearance or disappearance in the ordered or disordered phases can justify the existence of these phases. On the other

hand, Fermi-surface configurations and single-particle spectra in the α and β phases are different from the normal-state Fermi liquids. If the angle-resolved photon emission spectroscopy experiment can be performed, it can readily tell these phases. In the β phase, the order parameter is similar to the Rashba SO coupling, and the method to detect the Rashba coupling can be applied here. For example, from the beat pattern of the Shubnikov–de Haas oscillations of the $\rho(B)$, we can determine the spin splitting of two helicity bands. The asymmetry of the confining potential certainly will also contribute some part to the final spin-orbit coupling. However, when the dynamically generated part dominates, it will not be sensitive to the asymmetry of the confining potential.

XII. CONCLUSIONS

In summary, we have studied the Pomeranchuk instability involving spin in the high orbital partial-wave channels. GL free energies are constructed to understand the ordered phase patterns after the instabilities take place. The ordered phases can be classified into α and β phases as an analogy to the superfluid ^{3}He A and B phases. Both phases are characterized by a certain type of effective SO coupling, giving rise to a mechanism that generates SO couplings in a nonrelativistic systems. In the α phase, the Fermi surfaces exhibit an anisotropic distortion, while those in the β phase still keep the circular or spherical shapes undistorted. We further analyze the collective modes in the ordered phases at the RPA level. Similar to the Pomeranchuk instability in the spin-singlet density channel, the density channel Goldstone modes in the α phase also show anisotropic overdamping, except along some specific symmetry-determined directions. The spin channel Goldstone modes are found to exhibit nearly isotropic linear dispersion relations at small propagating wave vectors. The Goldstone modes in the β phase are relative spin-orbit rotation modes with linear dispersion relation at $l \geq 2$. The spin-wave modes in both ordered α and β phases couple to the Goldstone modes, which thus develop characteristic resonance peaks, which can be observed in inelastic neutron-scattering experiments. The p-wave channel is special in that the β phase can develop a spontaneous chiral Lifshitz instability in the originally nonchiral systems. The GL analysis was performed to obtain the twist pattern in the ground state. We also review the current experiment status for searching these instabilities in various systems, including ^{3}He, the heavy fermion compound URu_2Si_2, the bilayer ruthenate $Sr_3Ru_2O_7$, 2D electron gases, and p-wave Feshbach resonances with cold fermionic atoms. The $Sr_3Ru_2O_7$ seems to be the most promising system to exhibit such an instability in the 2D d-wave channel. However, investigation on the SO coupling effect is needed to understand the suppression of the resistivity anomaly due to the in-plane field.

There are still many important properties of the spin-triplet Pomeranchuk instabilities yet to be explored. In this paper, we did not discuss the behavior of the fermionic degrees of freedom, which are expected to be strongly anomalous. Generally speaking, the overdamped density channel

Goldstone modes in the α phase strongly couple to the fermions, which is expected to lead to a non-Fermi-liquid behavior as in the case of the density channel Pomeranchuk instabilities.[4,17] However, the Goldstone modes in the β phase are not damped as $l \geq 2$; thus, similar to the case of itinerant ferromagnets, the β phase remains a Fermi liquid. The p-wave channel is particularly interesting. We have shown in Eq. (2.12) that p-wave paramagnon fluctuations couple to fermions as a SU(2) gauge field. The linear derivative terms in the GL free energy also become relevant in the finite temperature non-Gaussian regime. The Hertz-Mills-type critical theory for the F_l^a contains other features not present in the ferromagnetic ones. We defer to a future publication to address the above interesting questions.

APPENDIX A: LANDAU INTERACTION PARAMETERS

Landau-Fermi liquid theory is characterized by the interaction functions, which describe the forward scattering process between quasiparticles as

$$f_{\alpha\beta,\gamma\delta}(\vec{p},\vec{p}') = f^s(\vec{p},\vec{p}') + f^a(\vec{p},\vec{p}')\vec{\sigma}_{\alpha\beta} \cdot \vec{\sigma}_{\gamma\delta}, \quad (A1)$$

where $\vec{p}$ and $\vec{p}'$ lie close to the Fermi surface. The expressions of f^s and f^a can be obtained through a general microscopic two-body SU(2) invariant interaction,

$$V(\vec{r}_1,\vec{r}_2) = V_c(\vec{r}_1 - \vec{r}_2) + V_s(\vec{r}_1 - \vec{r}_2)\vec{S}_1 \cdot \vec{S}_2, \quad (A2)$$

where the V_c and V_s are the spin-independent and -dependent parts, respectively. At the Hartree-Fock level, $f^{s,a}(p,p')$ are

$$f^s(\vec{p},\vec{p}') = V_c(0) - \frac{1}{2}V_c(\vec{p} - \vec{p}') - \frac{3}{8}V_s(\vec{p} - \vec{p}'),$$

$$f^a(\vec{p},\vec{p}') = -\frac{1}{2}V_c(\vec{p} - \vec{p}') + \frac{1}{4}V_s(0) + \frac{1}{8}V_s(\vec{p} - \vec{p}').$$

$$(A3)$$

$f^{s,a}(\vec{p},\vec{p}')$ can be further decomposed into different orbital angular momentum channels as

$$f_l^{s,a}$$

$$= \begin{cases} \displaystyle\int_{-1}^{1} d\cos\theta\, f^{s,a}(\hat{p}\cdot\hat{p}') P_l(\hat{p}\cdot\hat{p}') & \text{in three dimensions,} \\[12pt] \displaystyle\int (d\phi/2\pi) f^{s,a}(\hat{p}\cdot\hat{p}')\cos l\phi & \text{in two dimensions,} \end{cases}$$

(A4)

where P_l is the lth-order Legendre polynomial. For each channel of $F_l^{s,a}$, LP instability[3] occurs at

$$F_l^{s,a} = N(0) f_l^{s,a} \begin{cases} < -(2l+1) & \text{in three dimensions,} \\ < -(2 - \delta_{l,0}) & \text{in two dimensions,} \end{cases}$$

(A5)

where $N(0)$ is the density of states at the Fermi energy.

APPENDIX B: GOLDSTONE MODES OF THE SPIN OSCILLATION IN THE α PHASE

In this section, we calculate the spin channel Goldstone modes in the 2D α phases at small wave vector, $v_F q/\bar{n} \ll 1$, and low frequency, $\omega/\bar{n} \ll 1$. The expression for the dispersion of $L_{x\pm iy,1}(\vec{q},\omega)$ is

$$L_{x+iy,1}(\vec{q},\omega) = \kappa q^2 + \frac{1}{|f_1^a|} + 2\int \frac{d^2k}{(2\pi)^2} \cos^2 l\theta_k$$
$$\times \frac{n_f\left[\xi_l\left(\vec{k}-\frac{\vec{q}}{2}\right)\right] - n_f\left[\xi_\downarrow\left(\vec{k}+\frac{\vec{q}}{2}\right)\right]}{\omega + i\eta + \xi_\downarrow\left(\vec{k}-\frac{\vec{q}}{2}\right) - \xi_\uparrow\left(\vec{k}+\frac{\vec{q}}{2}\right)},$$

(B1)

where $\xi_{\uparrow,\downarrow}(k) = \epsilon(k) - \mu \mp \bar{n}\cos l\theta_k$. Following the procedure

in Ref. [4], we separate Eq. (B1) into a static part, $L_{x+iy,1}(\vec{q},\omega)$, and a dynamic part, $M_{x+iy,1}(\vec{q},\omega)$, as

$$L_{x+iy,1}(\vec{q},\omega) = L_{x+iy,1}(\vec{q},0) + M_{x+iy,1}(\vec{q},\omega).$$

(B2)

At $\vec{q}=0$, $\omega=0$, from the self-consistent equation [Eq. (4.3)], the integral cancels the constant term $\frac{1}{|f_1^a|}$ as required by the Goldstone theorem. The detailed form of the static part at small but nonzero $\vec{q}$ is difficult to evaluate due to anisotropic Fermi surfaces. Because of the breaking of parity in the α phase, it seems that the leading-order contribution should be linear to q. However, from the Ginzburg-Landau analysis in Sec. VII A, the linear derivative term in Eq. (3.5) does not contribute to the coupling among Goldstone modes, i.e., the uniform ground state is stable, in contrast to the case in the β phase. As a result, the dependence on $\vec{q}$ should start from the quadratic order, bringing a correction to the coefficient κ. For simplicity, we neglect this correction for it does not cause a qualitatively different result. Thus, we arrive at

$$L_{x+iy,1}(\vec{q},\omega=0) = \kappa q^2.$$

(B3)

The dynamic part, $M_{x+iy,1}(\vec{q},\omega)$, can be expressed as

$$M_{x+iy,1} = -2\int \frac{d^2k}{(2\pi)^2} \frac{\omega \cos^2 l\theta_k}{\omega + i\eta + \xi_\downarrow\left(\vec{k}-\frac{\vec{q}}{2}\right) - \xi_\uparrow\left(\vec{k}+\frac{\vec{q}}{2}\right)}$$
$$\times \frac{n_f\left[\xi_\downarrow\left(\vec{k}-\frac{\vec{q}}{2}\right)\right] - n_f\left[\xi_\uparrow\left(\vec{k}+\frac{\vec{q}}{2}\right)\right]}{\xi_\downarrow\left(\vec{k}-\frac{\vec{q}}{2}\right) - \xi_\uparrow\left(\vec{k}+\frac{\vec{q}}{2}\right)}.$$

(B4)

To evaluate this integral, we make several simplifications: the nonlinear part in $\epsilon(\vec{k})$ is neglected and the linear order in $\vec{q}$ is kept in the denominator. We arrive at

$$\int \frac{d\theta_k}{2\pi} \frac{\cos^2 l\theta_k}{\omega + i\eta + 2\bar{n}\cos l\theta_k - qv_F\cos(\theta_k - \phi)} \frac{-\omega}{2\bar{n}\cos l\theta_k - qv_F\cos(\theta_k - \phi)} \int \frac{kdk}{2\pi} \left\{ n_f\left[\xi_\downarrow\left(\vec{k}-\frac{\vec{q}}{2}\right)\right] - n_f\left[\xi_\uparrow\left(\vec{k}+\frac{\vec{q}}{2}\right)\right] \right\}$$
$$= \int \frac{d\theta_k}{2\pi} \frac{-\omega\cos^2 l\theta_k}{\omega + i\eta + 2\bar{n}\cos l\theta_k - qv_F\cos(\theta_k - \phi)} \frac{k_2^2 - k_1^2}{2\pi[2\bar{n}\cos l\theta_k - qv_F\cos(\theta_k - \phi)]},$$

(B5)

where k_1 and k_2 satisfy $n_f[\xi_\uparrow(\vec{k}_1+\vec{q}/2)]=0$ and $n_f[\xi_\downarrow(\vec{k}_2 -\vec{q}/2)]=0$, respectively, and ϕ is the azimuthal angle of $\vec{q}$. k_1 and k_2 can be approximated by

$$k_{1,2} = k_F\left(1 - \frac{x^2}{4}\right) \pm \left[\frac{\bar{n}\cos l\theta_k}{v_F} - \frac{q}{2}\cos(\theta_k - \phi)\right] + O(q^2).$$

(B6)

We now transfer the integral over θ_k to an integral over $z=\exp(i\theta_k)$ and define the density of the states at chemical potential in the ordered state as

$$N_<(0) = \frac{k_F(1 - x^2/4)}{v_F\pi}.$$

(B7)

The integral above now reads as

$$\frac{N_<(0)}{2\pi i} \oint \frac{dz}{z} \left(\frac{z^l + z^{-l}}{2}\right)^2 \frac{\omega}{\omega + i\eta + 2\bar{n}\dfrac{z^l + z^{-l}}{2} - \dfrac{qv_F}{2}(ze^{-i\phi} + z^{-1}e^{i\phi}) + O(q^2)}$$

$$\approx \frac{N_<(0)\omega}{4} \sum_{|z|<1} \text{Res}\left\{\frac{(z^l + z^{-l})^2}{z[2\omega + 2i\eta + 2\bar{n}(z^l + z^{-l}) - qv_F(ze^{-i\phi} + z^{-1}e^{i\phi})]}\right\}. \tag{B8}$$

This integral can be calculated by evaluating the residues at poles inside the unit circle. There is one pole at 0, one pole at ∞, and $2l$ poles, from the solutions of the equation:

$$2\omega + 2i\eta + 2\bar{n}(z^l + z^{-l}) - qv_F(ze^{-i\phi} + z^{-1}e^{i\phi}) = 0. \tag{B9}$$

The pole at $z=\infty$ is not inside the unit circle and does not contribute to the integral.

The pole at $z=0$ has different behaviors for different values of l. The residue is $-\frac{2\omega}{(2\bar{n} - e^{i\phi}qv_F)^2}$ for $l=1$, $-\frac{(4\bar{n}\omega - e^{2i\phi}q^2 v_F^2)}{8\bar{n}^3}$ for $l=2$, and $-\frac{\omega}{2\bar{n}^2}$ for all $l>2$. To the leading order, all the residues become $-\frac{\omega}{2\bar{n}^2}$ at $l \geq 1$. Next, we discuss the poles at the solutions of Eq. (B9). For $l \geq 1$, not all of these poles are located inside the unit circle. However, we will not bother to tell which poles are inside the unit circle because we can show that these poles at most only give negligible higher-order terms. In the limit of small q and ω, Eq. (B9) can be solved perturbatively as a power series of q and ω as $z_m = \exp[i(2m-1)\pi/2l] + O(q) + O(\omega)$, where $m = 1, 2, \ldots, 2l$. To the leading order, this type of poles are all simple poles, and the residue of $1/[2\omega + 2i\eta + 2\bar{n}(z^l + z^{-l}) - qv_F(ze^{-i\phi} + z^{-1}e^{i\phi})]$ is at the order of $O(\frac{1}{2\bar{n}})$. Therefore, the contribution from the pole z_m is

$$\frac{N_<(0)\omega}{4}\text{Res}\left[\frac{1}{z}\frac{(z^l + z^{-l})^2}{2\omega + 2i\eta + 2\bar{n}(z^l + z^{-l}) - qv_F(ze^{-i\phi} + z^{-1}e^{i\phi})}\right]_{z=z_m} \approx \frac{N_<(0)\omega}{2}\frac{[2\omega + 2i\eta - qv_F(z_m e^{-i\phi} + z_m^{-1}e^{i\phi})]^2}{z_m(2\bar{n})^2}\frac{1}{4l\bar{n}z_m^{l-1}}$$

$$\approx O\left[\frac{\omega(\omega + q)^2}{\bar{n}^3}\right], \tag{B10}$$

which is negligible to orders of $O(\omega^2/\bar{n}^2)$ and $O(q^2/\bar{n}^2)$.

In short, for $l \geq 1$, only the pole at $z=0$ contributes to the integral. The result of the fluctuation kernel is

$$L_{x+iy,1}(\vec{q}, \omega) = \kappa q^2 - \frac{N_<(0)}{4\bar{n}^2}\omega^2. \tag{B11}$$

From the self-consistent equation, we find that $N_<(0) = 2/|f_l^a|$. Therefore, the spin channel Goldstone mode reads

$$L_{x+iy,1}(\vec{q}, \omega) = \kappa q^2 - \frac{\omega^2}{2\bar{n}^2|f_l^a(0)|} = \kappa q^2 - \frac{N(0)}{2|F_l^a|}\frac{\omega^2}{\bar{n}^2}, \tag{B12}$$

at $l \geq 1$.

[1] A. J. Leggett, Rev. Mod. Phys. **47**, 331 (1975).

[2] G. Baym and C. Pethick, *Landau Fermi-liquid Theory* (Wiley, New York, 1984).

[3] I. I. Pomeranchuk, Sov. Phys. JETP **8**, 361 (1959).

[4] V. Oganesyan, S. A. Kivelson, and E. Fradkin, Phys. Rev. B **64**, 195109 (2001).

[5] P. G. de Gennes and J. Prost, *The Physics of Liquid Crystals*, 2nd ed. (Clarendon Press, Oxford, 1993).

[6] P. M. Chaikin and T. C. Lubensky, *Principles of Condensed Matter Physics* (Cambridge University Press, Cambridge, 1995).

[7] S. A. Kivelson, E. Fradkin, and V. J. Emery, Nature (London) **393**, 550 (1998).

[8] S. A. Kivelson, I. P. Bindloss, E. Fradkin, V. Oganesyan, J. M. Tranquada, A. Kapitulnik, and C. Howald, Rev. Mod. Phys. **75**, 1201 (2003).

[9] E. Fradkin and S. A. Kivelson, Phys. Rev. B **59**, 8065 (1999).

[10] E. Fradkin, S. A. Kivelson, E. Manousakis, and K. Nho, Phys. Rev. Lett. **84**, 1982 (2000).

[11] M. P. Lilly, K. B. Cooper, J. P. Eisenstein, L. N. Pfeiffer, and K. W. West, Phys. Rev. Lett. **82**, 394 (1999).

[12] K. B. Cooper, M. P. Lilly, J. P. Eisenstein, L. N. Pfeiffer, and K. W. West, Phys. Rev. B **65**, 241313(R) (2002).

[13] R. R. Du, D. C. Tsui, H. L. Stormer, L. N. Pfeiffer, K. W. Baldwin, and K. W. West, Solid State Commun. **109**, 389 (1999).

[14] S. A. Grigera, P. Gegenwart, R. A. Borzi, F. Weickert, A. J. Schofield, R. S. Perry, T. Tayama, T. Sakakibara, Y. Maeno, A. G. Green, and A. P. Mackenzie, Science **306**, 1154 (2004).

[15] R. A. Borzi, S. A. Grigera, J. Farrell, R. S. Perry, S. J. S. Lister, S. L. Lee, D. A. Tennant, Y. Maeno, and A. P. Mackenzie, Science **315**, 214 (2007).

[16] D. G. Barci and L. E. Oxman, Phys. Rev. B **67**, 205108 (2003).

[17] M. J. Lawler, D. G. Barci, V. Fernandez, E. Fradkin, and L. Oxman, Phys. Rev. B **73**, 085101 (2006).

[18] J. Nilsson and A. H. Castro Neto, Phys. Rev. B **72**, 195104 (2005).

[19] J. Quintanilla and A. J. Schofield, Phys. Rev. B **74**, 115126 (2006).

[20] C. J. Halboth and W. Metzner, Phys. Rev. Lett. **85**, 5162 (2000).

[21] L. Dell'Anna and W. Metzner, Phys. Rev. B **73**, 045127 (2006).

[22] H. Y. Kee, Phys. Rev. B **67**, 073105 (2003).

[23] I. Khavkine, C. H. Chung, V. Oganesyan, and H. Y. Kee, Phys. Rev. B **70**, 155110 (2004).

[24] H. Yamase, V. Oganesyan, and W. Metzner, Phys. Rev. B **72**, 035114 (2005).

[25] S. A. Kivelson, E. Fradkin, and T. H. Geballe, Phys. Rev. B **69**, 144505 (2004).

[26] M. J. Lawler and E. Fradkin Phys. Rev. B **75**, 033304 (2007).

[27] J. E. Hirsch, Phys. Rev. B **41**, 6820 (1990).

[28] J. E. Hirsch, Phys. Rev. B **41**, 6828 (1990).

[29] L. P. Gorkov and A. Sokol, Phys. Rev. Lett. **69**, 2586 (1999).

[30] C. J. Wu and S. C. Zhang, Phys. Rev. Lett. **93**, 036403 (2004).

[31] C. M. Varma, Philos. Mag. **85**, 1657 (2005).

[32] C. M. Varma and L. J. Zhu, Phys. Rev. Lett. **96**, 036405 (2006).

[33] H. Y. Kee and Y. B. Kim, Phys. Rev. B **71**, 184402 (2005).

[34] C. Honerkamp, Phys. Rev. B **72**, 115103 (2005).

[35] D. Podolsky and E. Demler, New J. Phys. **7**, 59 (2005).

[36] J. Zaanen and Z. Nussinov, Phys. Status Solidi B **236**, 332 (2003).

[37] In this paper, we consider only the effects of charge and spin degrees of freedom. Thus, "orbital" effects refer here only to channels with nonzero orbital angular momentum l. These are *not* the orbital degrees of freedom of multiband models commonly used in ruthenate and manganite materials. Throughout this paper, we consider systems in which the conduction electrons correspond only to one effective band.

[38] B. A. Bernevig, J. Orenstein, and S. C. Zhang, Phys. Rev. Lett. **97**, 236601 (2006).

[39] S. Murakami, N. Nagaosa, and S. C. Zhang, Science **301**, 1348 (2003).

[40] J. Sinova, D. Culcer, Q. Niu, N. A. Sinitsyn, T. Jungwirth, and A. H. MacDonald, Phys. Rev. Lett. **92**, 126603 (2004).

[41] Y. K. Kato, R. C. Myers, A. C. Gossard, and D. D. Awschalom, Phys. Rev. Lett. **93**, 176601 (2004).

[42] J. Wunderlich, B. Kaestner, J. Sinova, and T. Jungwirth, Phys. Rev. Lett. **94**, 047204 (2005).

[43] B. Binz, A. Vishwanath, and V. Aji, Phys. Rev. Lett. **96**, 207202 (2006).

[44] J. A. Hertz, Phys. Rev. B **14**, 1165 (1976).

[45] A. J. Millis, Phys. Rev. B **48**, 7183 (1993).

[46] D. Vollhardt and P. Wolfle, *The Superfluid Phases of Helium 3* (Taylor & Francis, London, 1990).

[47] H. Y. Kee, E. H. Kim, and C. H. Chung, Phys. Rev. B **68**, 245109 (2003).

[48] H. Doh, N. Friedman, and H.-Y. Kee, Phys. Rev. B **73**, 125117 (2006).

[49] R. Winkler, Phys. Rev. B **62**, 4245 (2000).

[50] J. Schliemann and D. Loss, Phys. Rev. B **71**, 085308 (2005).

[51] P. McGraw, Phys. Rev. D **50**, 952 (2004).

[52] F. Zhou, Int. J. Mod. Phys. B **17**, 2643 (2003).

[53] C. Wu, J. P. Hu, and S. C. Zhang, cond-mat/0512602 (unpublished).

[54] A. S. Schwarz, Nucl. Phys. B **208**, 141 (1982).

[55] M. Bucher, H. K. Lo, and J. Preskill, Nucl. Phys. B **386**, 3 (1999).

[56] D. Belitz, T. R. Kirkpatrick, and T. Vojta, Rev. Mod. Phys. **77**, 579 (2005).

[57] H. v. Löhneysen, A. Rosch, M. Vojta, and P. Wolfle, cond-mat/0606317 (unpublished).

[58] E. Demler, W. Hanke, and S.-C. Zhang, Rev. Mod. Phys. **76**, 909 (2004).

[59] A. L. Fetter (private communication).

[60] Y. B. Kim (private communication).

[61] T. C. Lubensky and L. Radzihovsky, Phys. Rev. E **66**, 031704 (2002).

[62] A. P. Mackenzie and Y. Maeno, Rev. Mod. Phys. **75**, 657 (2003).

[63] A. J. Leggett, J. Phys. C **3**, 448 (1970).

[64] L. R. Corruccini, D. D. Osheroff, D. M. Lee, and R. C. Richards, Phys. Rev. Lett. **27**, 650 (1971).

[65] D. D. Osheroff, Physica B & C **90**, 20 (1977).

[66] D. S. Greywall, Phys. Rev. B **27**, 2747 (1983).

[67] V. Tripathi, P. Chandra, and P. Coleman, J. Phys.: Condens. Matter **17**, 5285 (2005).

[68] O. O. Bernal, C. Rodrigues, A. Martinez, H. G. Lukefahr, D. E. MacLaughlin, A. A. Menovsky, and J. A. Mydosh, Phys. Rev. Lett. **87**, 196402 (2001).

[69] R. Jamei, S. Kivelson, and B. Spivak, Phys. Rev. Lett. **94**, 056805 (2005).

[70] Y. Kwon, D. M. Ceperley, and R. M. Martin, Phys. Rev. B **50**, 1684 (1994).

[71] G. H. Chen and M. E. Raikh, Phys. Rev. B **60**, 4826 (1999).

[72] G.-H. Chen, M. E. Raikh, and Y.-S. Wu, Phys. Rev. B **61**, R10539 (2000).

[73] J. Zhang, E. G. M. van Kempen, T. Bourdel, L. Khaykovich, J. Cubizolles, F. Chevy, M. Teichmann, L. Tarruell, S. J. J. M. F. Kokkelmans, and C. Salomon, Phys. Rev. A **70**, 030702(R) (2004).